Conformational analysis of small organic molecules using NOE and RDC data: A discussion of strychnine and α-methylene-γ-butyrolactone - Supporting Information

Andreas Kolmer[a], Luke J. Edwards[b,c], Ilya Kuprov[d], Christina M. Thiele[a,*]

[a] *Clemens-Schöpf-Institut für Organische Chemie und Biochemie, Technische Universität Darmstadt, Alarich-Weiss-Straße 4, 64287 Darmstadt, Germany*
[b] *Department of Chemistry, University of Oxford, Inorganic Chemistry Laboratory, South Parks Road, Oxford, OX1 3QG, United Kingdom*
[c] *Current affiliation: Wellcome Trust Centre for Neuroimaging, UCL, 12 Queen Square, London, WC1N 3BG, United Kingdom*
[d] *School of Chemistry, Faculty of Natural and Environmental Sciences, University of Southampton, University Road, Southampton, SO17 1BJ, United Kingdom*

1. Experimental details

38.5 mg of strychnine **1** was dissolved in 960 μl $CDCl_3$ (120 mM). 1.5 mg of α-methylene-γ-butyrolactone **2** was dissolved in 490 μl D_2O (19 mM). Both samples were degassed using the freeze-pump-thaw method. Afterwards, the tubes were sealed in vacuo and stored at 277K.

The NOE measurements were recorded at 300K without sample spinning on a Bruker AVANCE III 600 spectrometer equipped with a 5 mm triple-resonance broadband inverse probe with z-gradient and a proton resonance frequency of 600.4 MHz. For the quantitative determination of distances via the NOE, first T_1 relaxation time constants were measured using the inversion-recovery method, which is available as *t1ir* in the Bruker pulse sequence library. The relaxation delays in the 1D PFGSE NOE experiment [1–3] with zero-quantum suppression [4–6] (available in the Bruker pulse sequence library as *selnogpzs*) were set accordingly to 15 s ($5 * T_1$ of the slowest relaxing group). For selective refocusing, a Gaussian pulse was chosen. The length of the Gaussian pulse was set to 80 ms, corresponding to an excitation bandwith of 9.2 Hz. For each distance to be determined, NOE experiments with mixing times from 50 to 400 ms in 25 ms-steps were recorded. The integral ratio of NOE peak to inverted peak was plotted against the mixing time and its slope was calculated using a linear fit (PANIC approach [7]).

2. Strong coupling

H_{23b} is strongly coupled to H_{23a}. When irradiating proton H_{23b} without zero-quantum-suppression (see figure SI.1), a modulation of both signals is visible. When zero-quantum suppression is used, the spectra look fine (see figure SI.2), but the corresponding PANIC plots still show an oscillation (see figure SI.3).

*Corresponding author
Email address: cthiele@thielelab.de (Christina M. Thiele)

3. WEEDHEAD

The self-written software used for the conformational analysis is called *WEEDHEAD Examines Experimental Distance Heretics from Ensemble Averaged Distances* (*WEEDHEAD*). It is written in *C*, and is available at the website of our group [8] under the license CC BY-NC-SA 4.0.

For the presented work, *WEEDHEAD* was used in version 0.9. The files used for the NOE analysis of strychnine **1** and α-methylene-γ-butyrolactone **2** are also available as example files for *WEEDHEAD*.

4. Aromatic protons

The aromatic protons of strychnine **1** show a behaviour that is not yet understood. This behaviour occurs in both experimental and simulated PANIC plots (see figures SI.4 and SI.5). This might be due to insufficient zero-quantum suppression; the behaviour observed, however, is different.

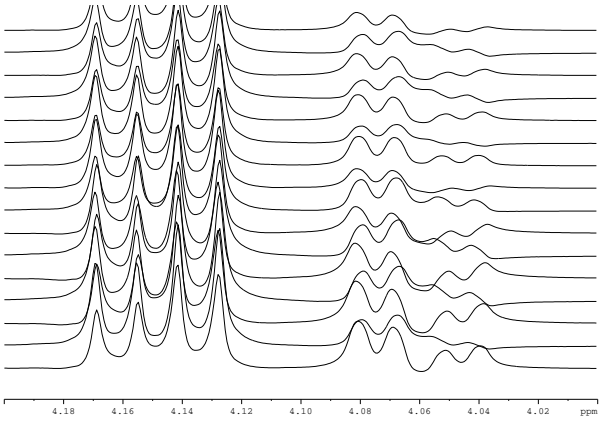

Figure SI.1: Irradiation at H_{23b} and detection at H_{23a} of strychnine **1** without zero-quantum suppression. The visible modulation results in the oscillation in the PANIC plots.

5. The determined distances

For strychnine **1**, we chose $H_{15a}-H_{15b}$ as calibration distance and set it to 1.760 Å. The analysis of $H_{15b}-H_{15a}$ then leads to a distance of 1.757 Å, which is in excellent agreement with the calibration distance. The difference of 0.003 Å was used as Δr_{ref} in equation SI.1, which was used to determine the errors of the determined distances.

Because some of the T_1-time constants differ significantly, we chose to use the relayed calibration as proposed by Butts et al.[9]. Starting at $H_{15a}-H_{15b}$, $H_{15b}-H_{15a}$ was used for irradiaton at H_{15b}. Next, $H_{13}-H_{15a}$ was used for irradiaton at H_{13}, $H_{16}-H_{15a}$ for H_{16} and H_1-H_{15a} for H_1. From $H_{20a}-H_{15b}$ for H_{20a} onwards to $H_{20b}-H_{20a}$ for H_{20b}, which continues to $H_{22}-H_{20b}$ for H_{22} and $H_{18b}-H_{20b}$ for H_{18b}.

From those we went on to $H_{23b}-H_{22}$ for H_{23b} and $H_{18a}-H_{18b}$ for H_{18a}. The last few calibration distances are H_8-H_{13} for H_8, $H_{12}-H_{13}$ for H_{12}, $H_{11b}-H_8$ for H_{11b} and $H_{23a}-H_{12}$ for H_{23a}.

For α-methylene-γ-butyrolactone **2**, we chose $H_{6a}-H_{6b}$ as calibration distance and set it to 1.886 Å. The analysis of $H_{6b}-H_{6a}$ then leads to a distance of 1.877 Å, which is in excellent agreement with the calibration distance. The difference of 0.009 Å was used as Δr_{ref} in equation SI.1, which was used to determine the errors of the determined distances. For the distances reported herein, this method gives errors of reasonable size. If very small signal-to-noise-ratios would be present, this method might underestimate the experimental errors.

To determine the distances between H_{6b} and H_3, the distances determined from $H_{6b}-H_3$ and H_3-H_{6b} were averaged. The same procedure was applied for the distance

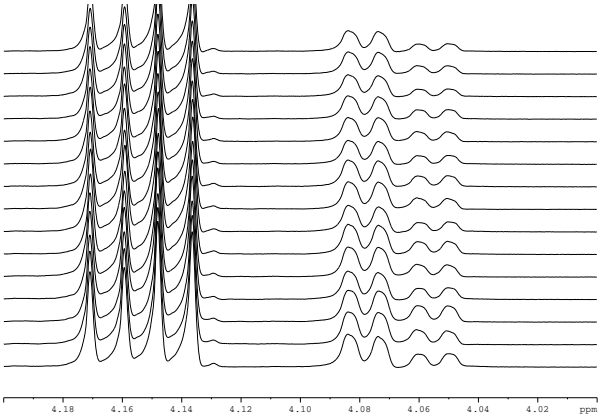

Figure SI.2: Irradiation at H_{23b} and detection at H_{23a} of strychnine **1** with zero-quantum suppression. There is no modulation visible, but there is still an oscillation in the PANIC plots.

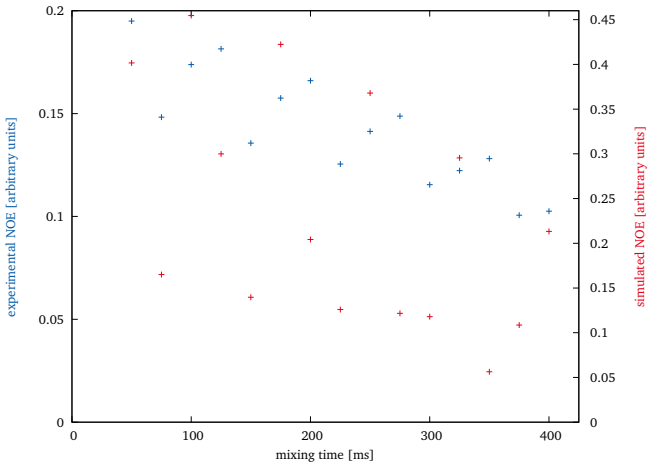

Figure SI.3: A comparison of experimental and simulated mixing time series for $H_{23b}-H_{23a}$ of strychnine **1** with zero-quantum suppression.

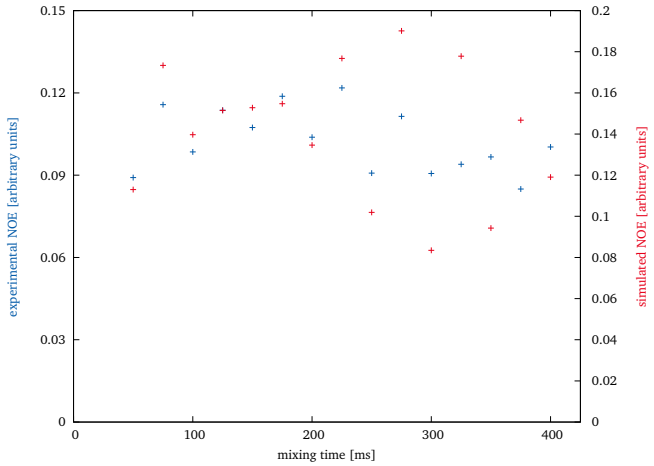

Figure SI.4: A comparison of experimental and simulated mixing time series for H_1-H_2 of strychnine **1** with zero-quantum suppression.

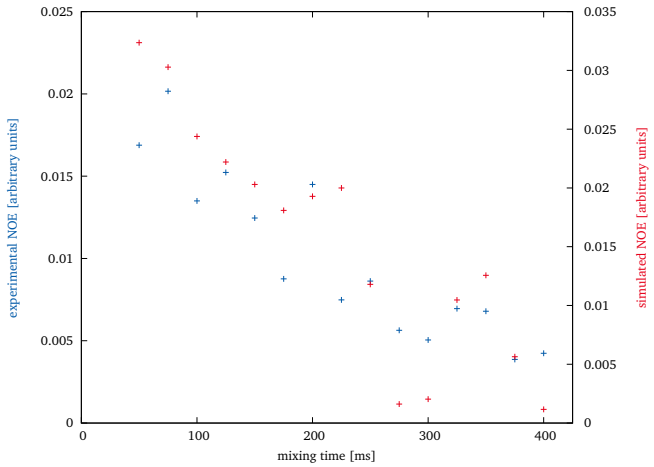

Figure SI.5: A comparison of experimental and simulated mixing time series for H_3-H_2 of strychnine **1** with zero-quantum suppression.

between H_2 and H_3. Because the T_1-times do not differ significantly, the relayed calibration is not necessary.

Table SI.1: The determined distances of strychnine **1**. See figure 1 of the main text for nomenclature.

proton 1	proton 2	distance/Å
H_{11b}	H_{23b}	3.596 ± 0.039
H_{11b}	H_8	2.536 ± 0.025
H_{11b}	H_{12}	2.959 ± 0.062
H_{11b}	H_{11a}	1.795 ± 0.018
H_{13}	H_{12}	2.244 ± 0.009
H_{13}	H_{11b}	3.788 ± 0.043
H_{13}	H_8	2.914 ± 0.028
H_{14}	H_{13}	2.251 ± 0.012
H_{15a}	H_1	3.734 ± 0.065
H_{15a}	H_{13}	2.188 ± 0.006
H_{15a}	H_8	4.220 ± 0.057
H_{15a}	H_{16}	2.464 ± 0.006
H_{15a}	H_{14}	2.493 ± 0.009
H_{15b}	H_{20a}	2.186 ± 0.008
H_{15b}	H_{14}	2.423 ± 0.024
H_{15b}	H_{16}	2.475 ± 0.011
H_{18a}	H_{16}	3.611 ± 0.061
H_{18a}	H_{20b}	2.748 ± 0.022
H_{18b}	H_{20b}	2.343 ± 0.011
H_{18b}	H_{16}	3.780 ± 0.078
H_{18b}	H_{18a}	1.691 ± 0.013
H_{20b}	H_{20a}	1.781 ± 0.007
H_{22}	H_{23a}	2.858 ± 0.042
H_{22}	H_{23b}	2.370 ± 0.014
H_{22}	H_{20b}	2.306 ± 0.010
H_8	H_{18b}	2.147 ± 0.023
H_{11b}	H_{23a}	4.254 ± 0.085
H_{20b}	H_{23b}	4.774 ± 0.077
H_{20b}	H_{16}	3.959 ± 0.030
H_{12}	H_{23a}	2.232 ± 0.009
H_{12}	H_8	3.480 ± 0.058
H_{16}	H_{20a}	3.320 ± 0.061
H_{16}	H_{13}	3.872 ± 0.026

Table SI.2: The determined distances of α-methylene-γ-butyrolactone **2**. See figure 1 of the main text for nomenclature.

proton 1	proton 2	distance/Å
H_{6b}	H_3	3.087 ± 0.026
H_2	H_3	3.083 ± 0.032
H_1	H_2	2.742 ± 0.017
H_1	H_3	2.831 ± 0.017

$$\Delta r_{IS} = \sqrt{\left(\frac{-r_{\mathrm{ref}}}{6\left(\frac{\sigma_{IS}}{\sigma_{\mathrm{ref}}}\right)^{\frac{7}{6}}\sigma_{\mathrm{ref}}} * \Delta\sigma_{IS}\right)^2 + \left(\frac{r_{\mathrm{ref}}\sigma_{IS}}{6\left(\frac{\sigma_{IS}}{\sigma_{\mathrm{ref}}}\right)^{\frac{7}{6}}\sigma_{\mathrm{ref}}^2} * \Delta\sigma_{\mathrm{ref}}\right)^2 + \left(\left(\frac{\sigma_{IS}}{\sigma_{\mathrm{ref}}}\right)^{-\frac{1}{6}} * \Delta r_{\mathrm{ref}}\right)^2} \quad \text{(SI.1)}$$

6. The validity of the initial-rate-approximation for strychnine 1

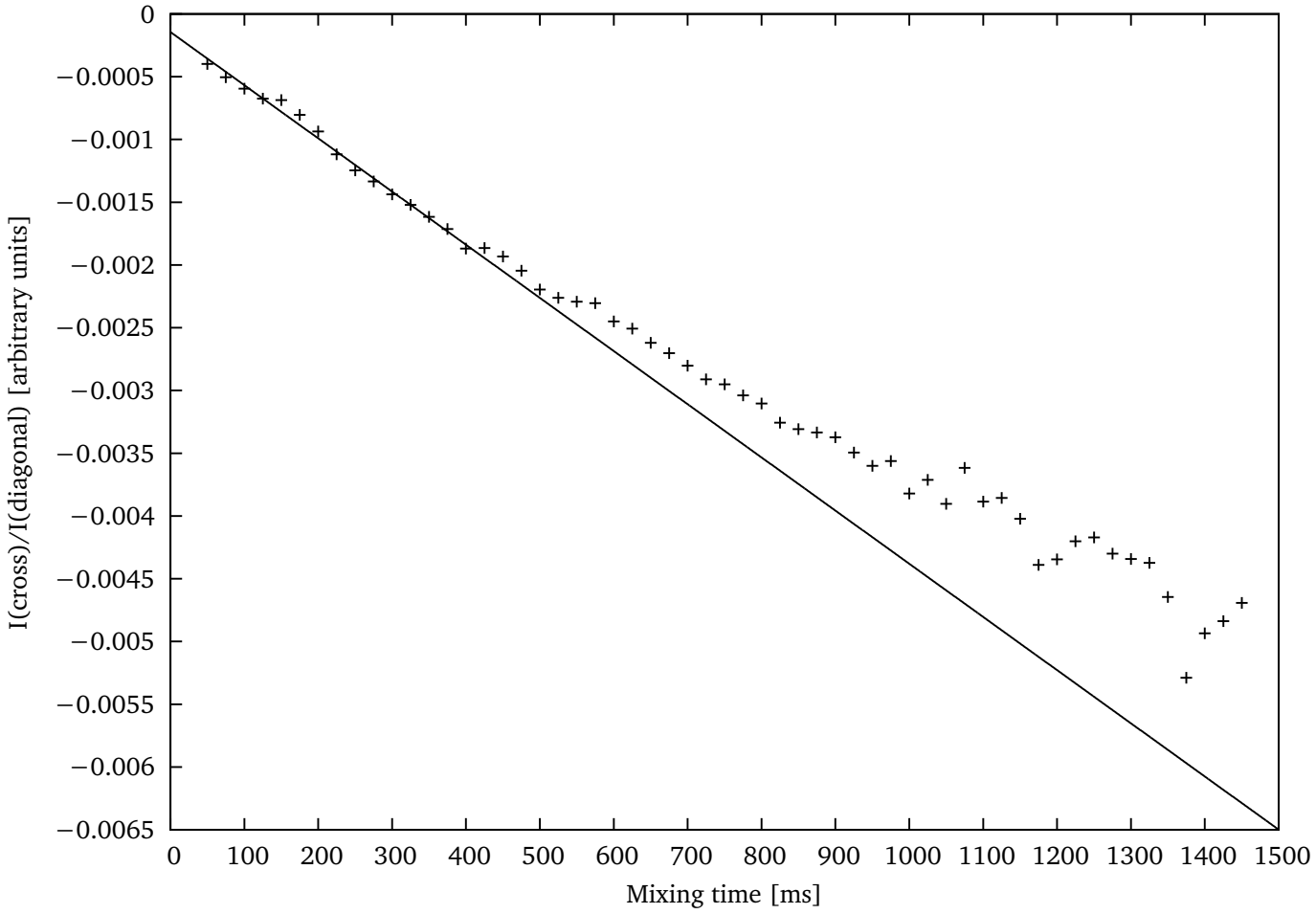

Figure SI.6: PANIC plot for $H_{11b}-H_{23b}$ of strychnine **1**, overlaid with the linear slope determined from the points from 50 - 400 ms. The initial-rate-approximation seems valid for mixing times up to 600 ms. After 1000 ms, phase correction problems occur, leading to a scattering of the data points.

7. PANIC plots for strychnine 1

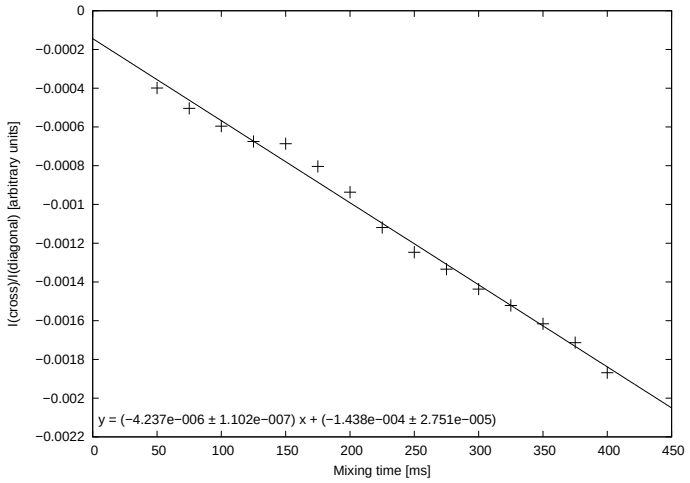

(a) H_{11b}−H_{23b}

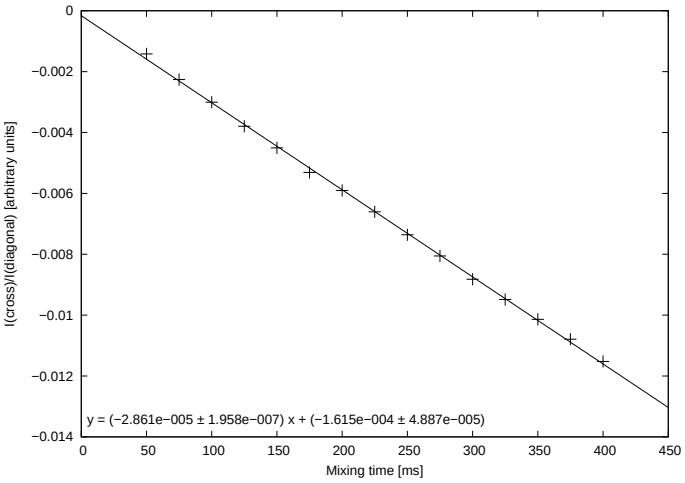

(b) H_{8}−H_{11b}

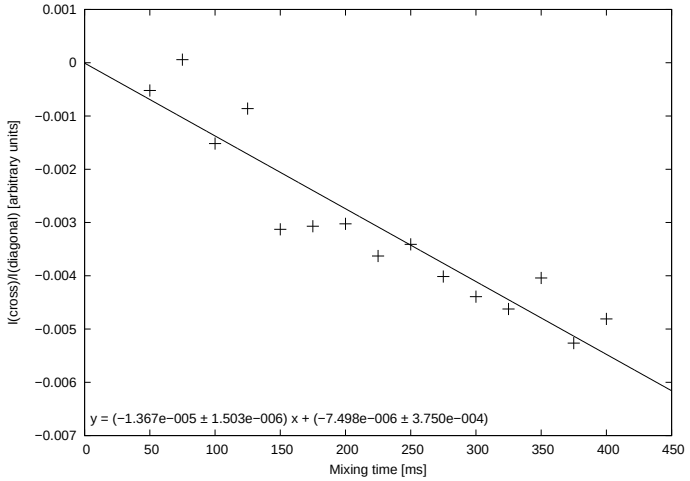

(c) H_{11b}−H_{12}

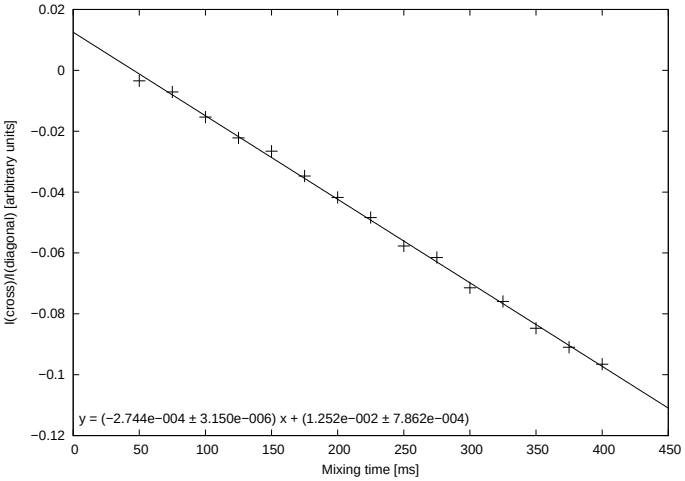

(d) H_{11b}−H_{11a}

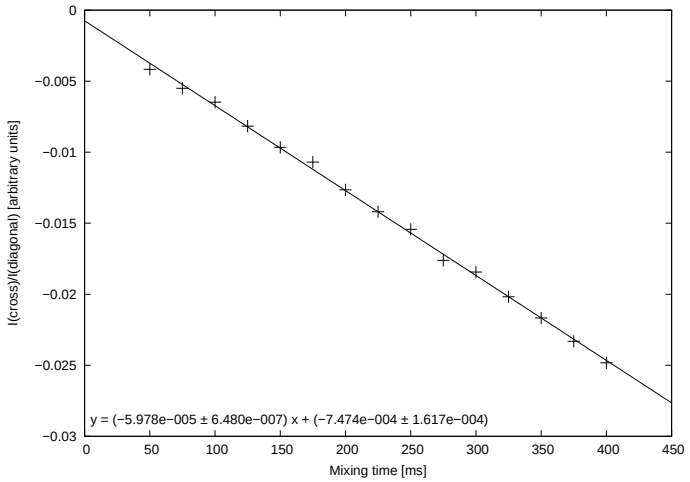

(e) H_{13}−H_{12}

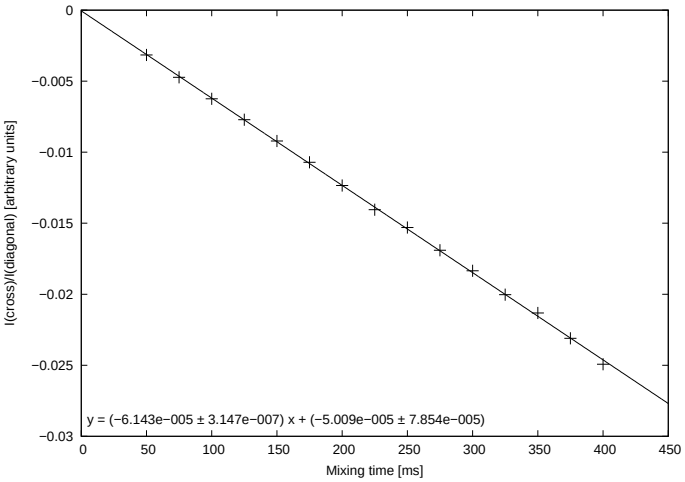

(f) H_{12}−H_{13}

Figure SI.7: The experimental PANIC plots for strychnine **1**.

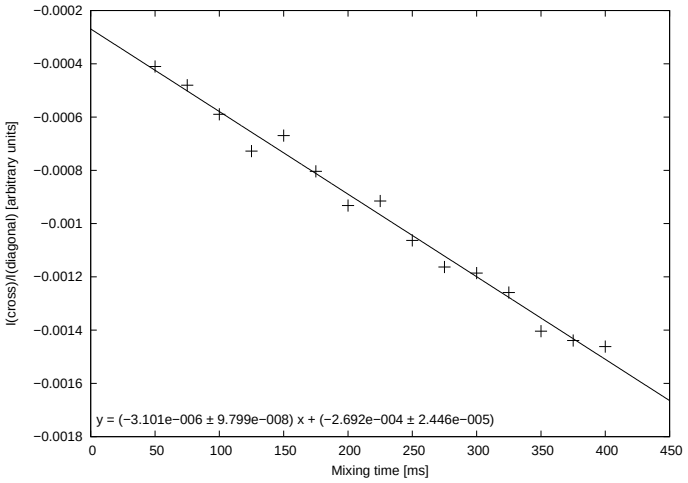

(g) H_{11b}−H_{13}

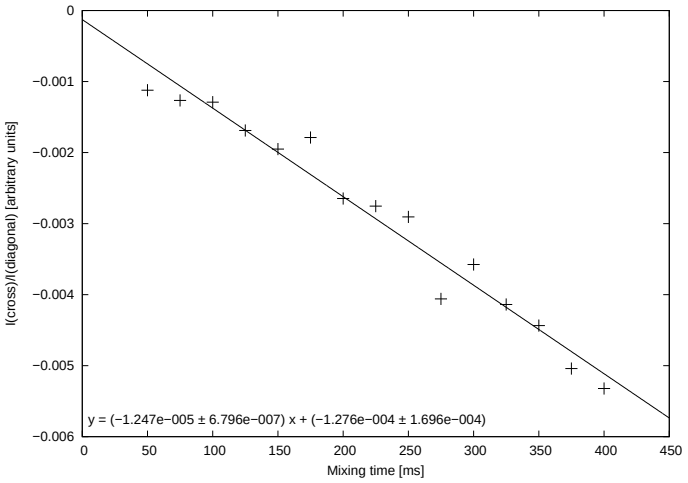

(h) H_{13}−H_{8}

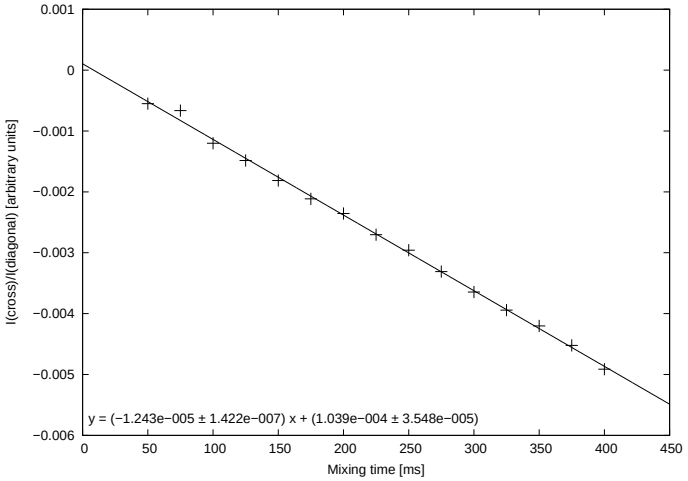

(i) H_{8}−H_{13}

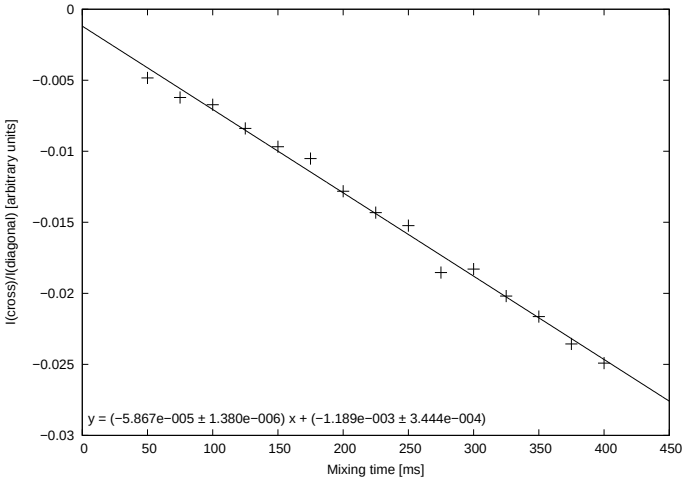

(j) H_{13}−H_{14}

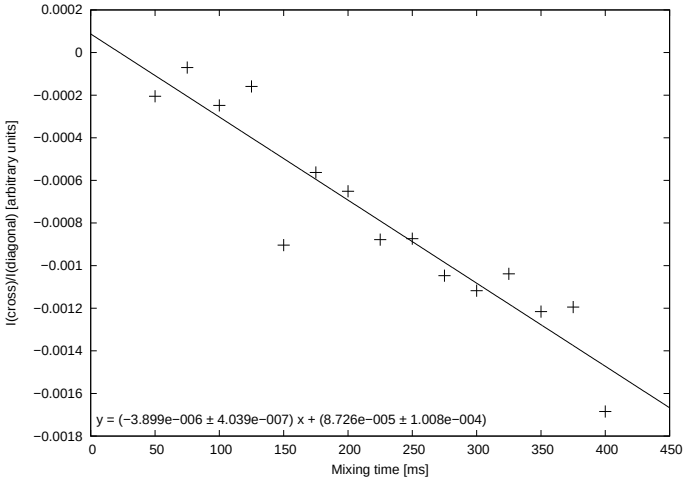

(k) H_{15a}−H_{1}

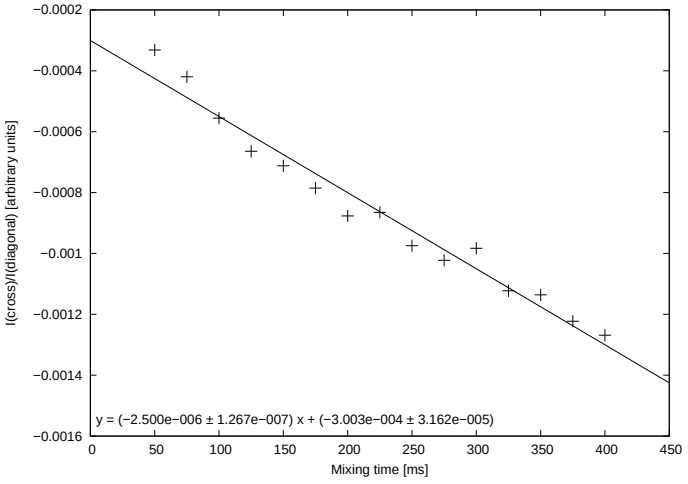

(l) H_{1}−H_{15a}

Figure SI.7: The experimental PANIC plots for strychnine **1**.

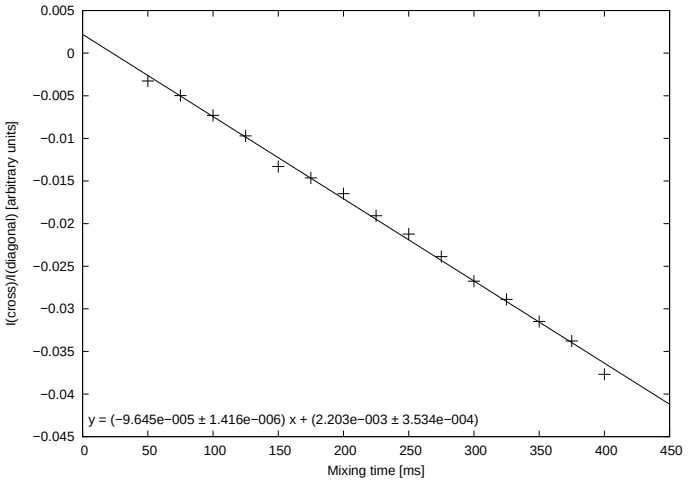

(m) H_{15a}−H_{13}

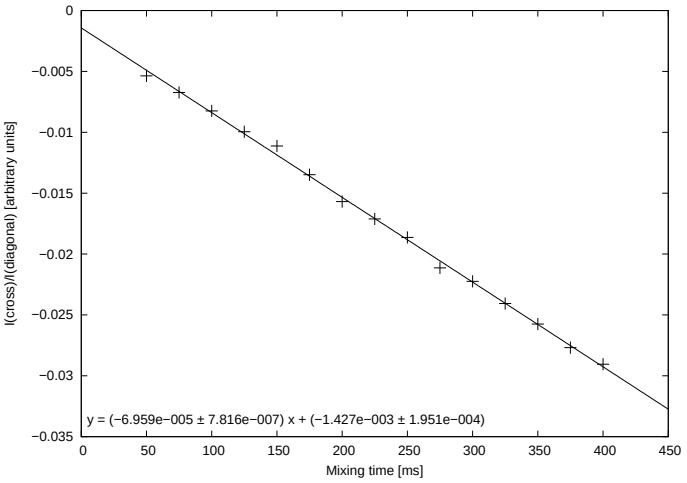

(n) H_{13}−H_{15a}

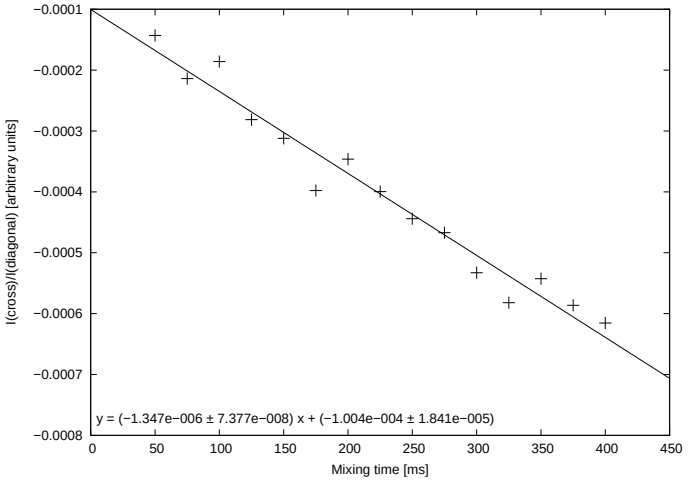

(o) H_{8}−H_{15a}

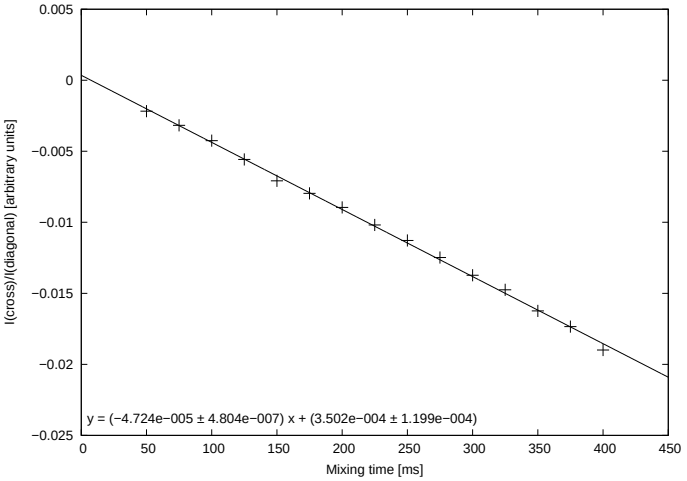

(p) H_{15a}−H_{16}

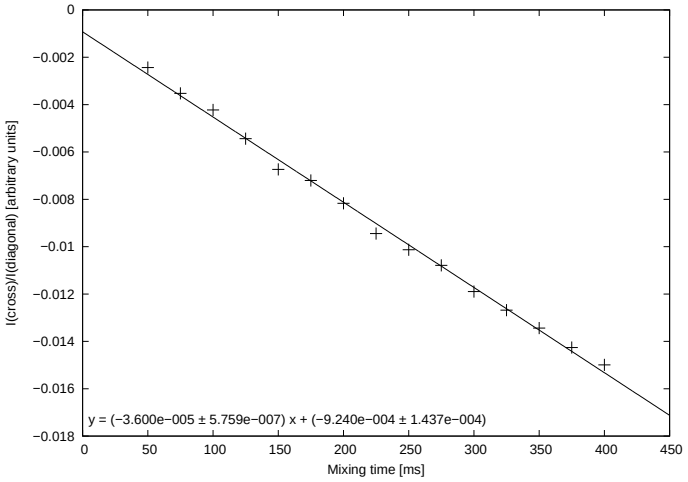

(q) H_{16}−H_{15a}

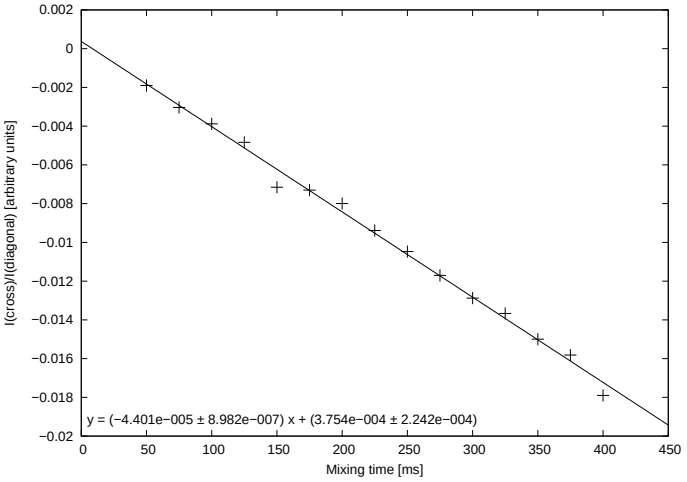

(r) H_{15a}−H_{14}

Figure SI.7: The experimental PANIC plots for strychnine **1**.

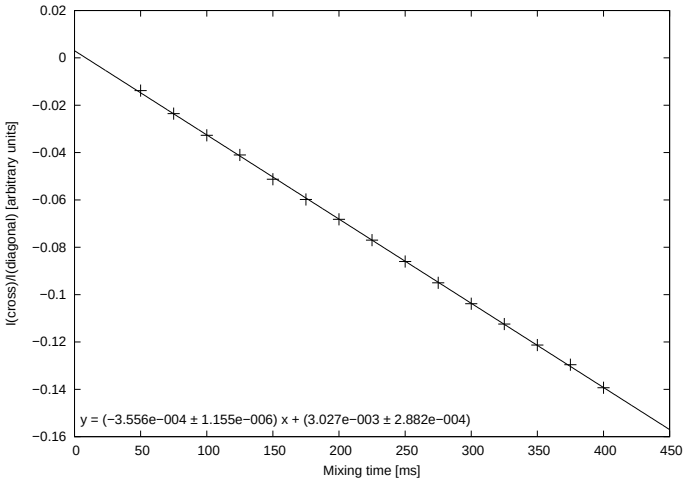

(s) H_{15a}−H_{15b} (used as reference distance)

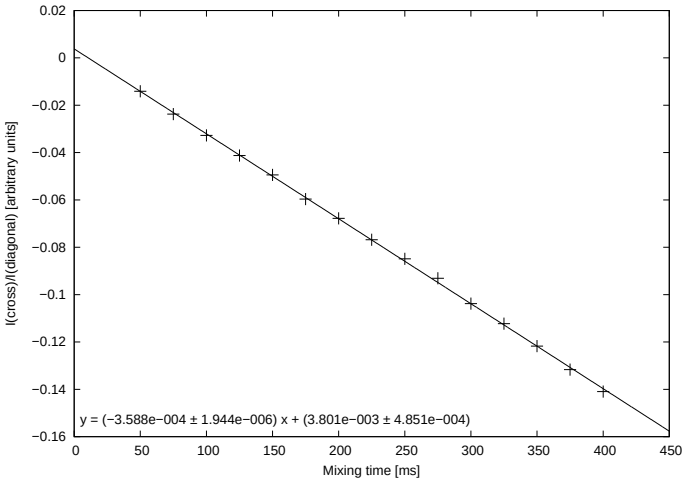

(t) H_{15b}−H_{15a}

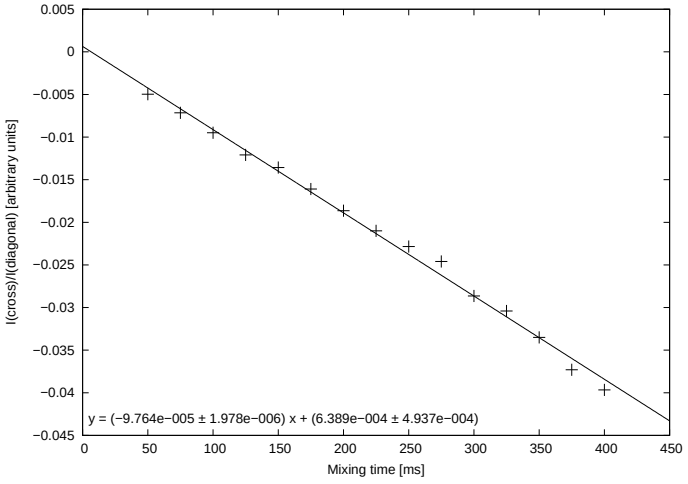

(u) H_{15b}−H_{20a}

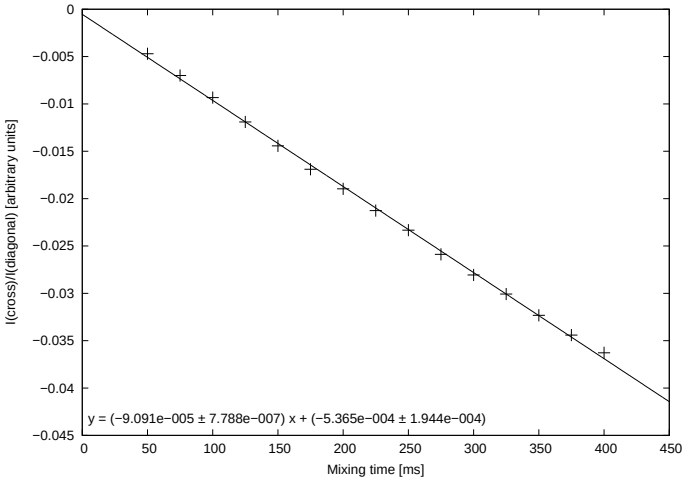

(v) H_{20a}−H_{15b}

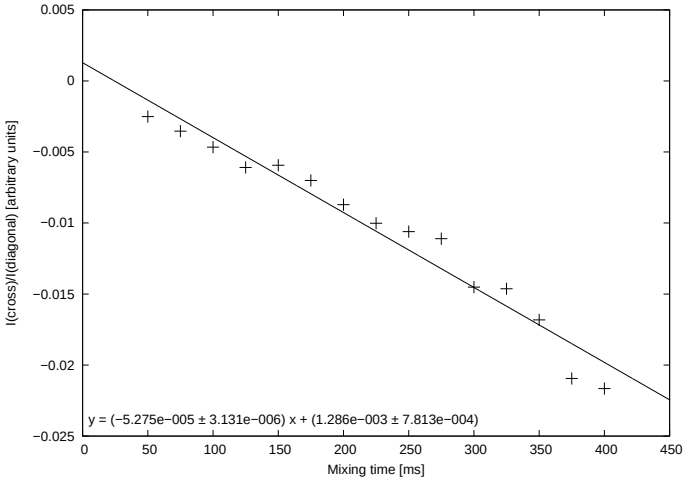

(w) H_{15b}−H_{14}

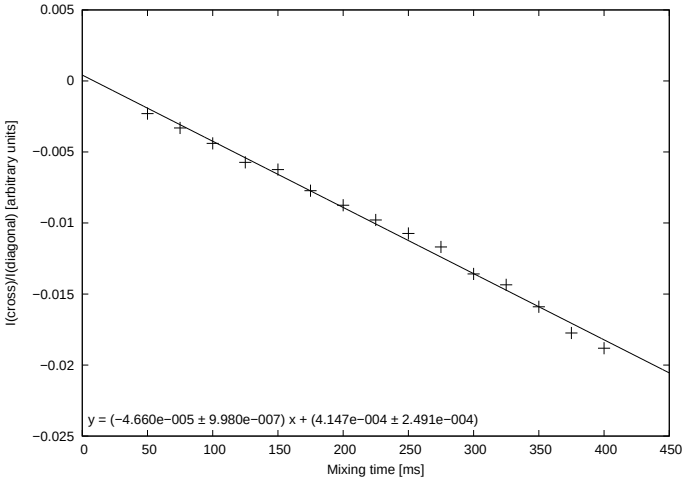

(x) H_{15b}−H_{16}

Figure SI.7: The experimental PANIC plots for strychnine **1**.

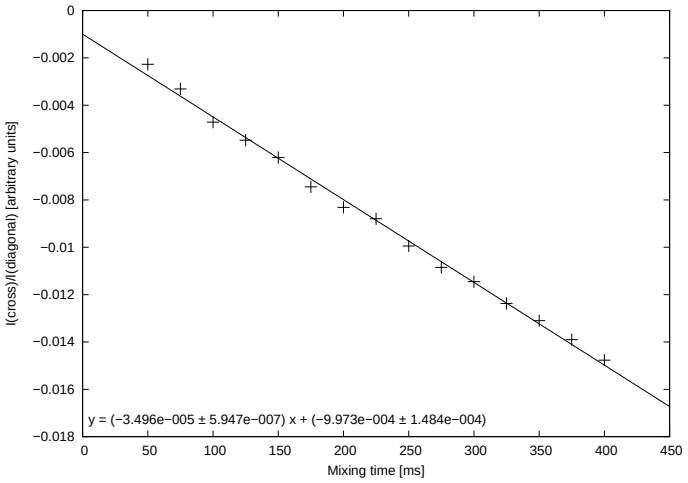

(y) H_{16}−H_{15b}

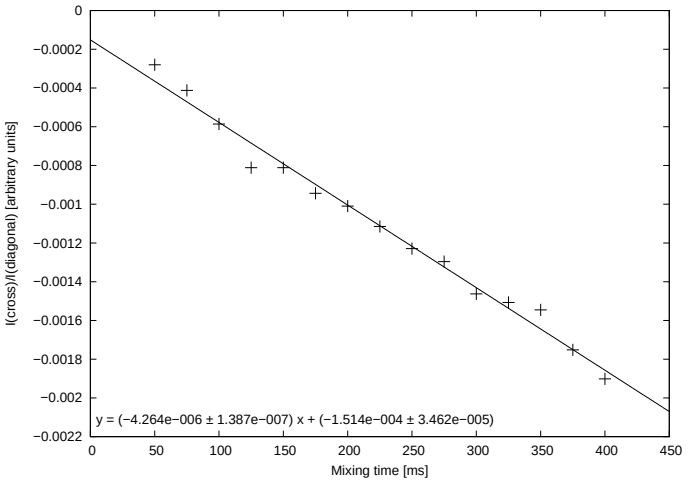

(z) H_{18a}−H_{16}

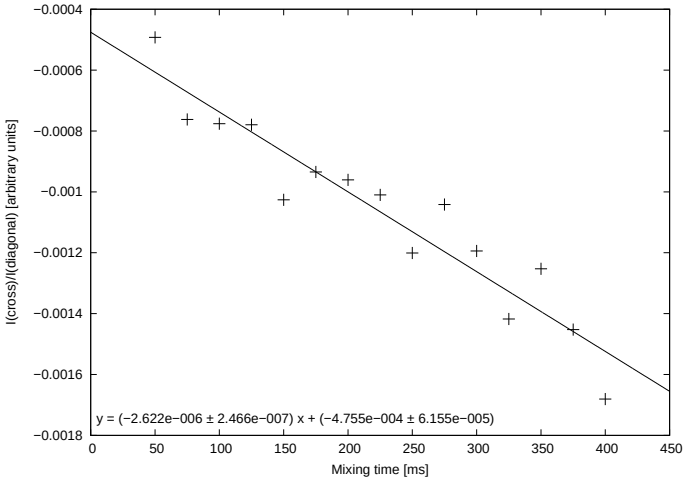

(aa) H_{16}−H_{18a}

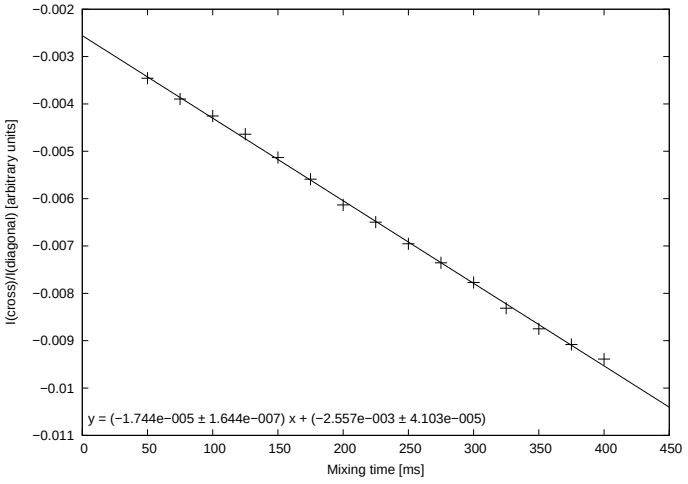

(ab) H_{18a}−H_{20b}

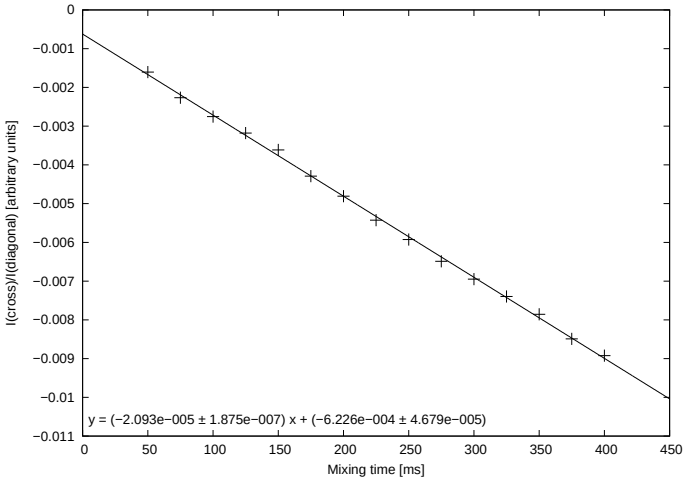

(ac) H_{20b}−H_{18a}

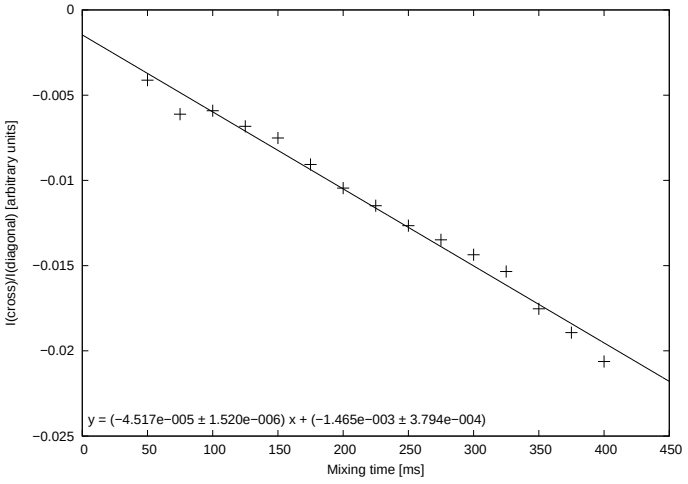

(ad) H_{18b}−H_{20b}

Figure SI.7: The experimental PANIC plots for strychnine **1**.

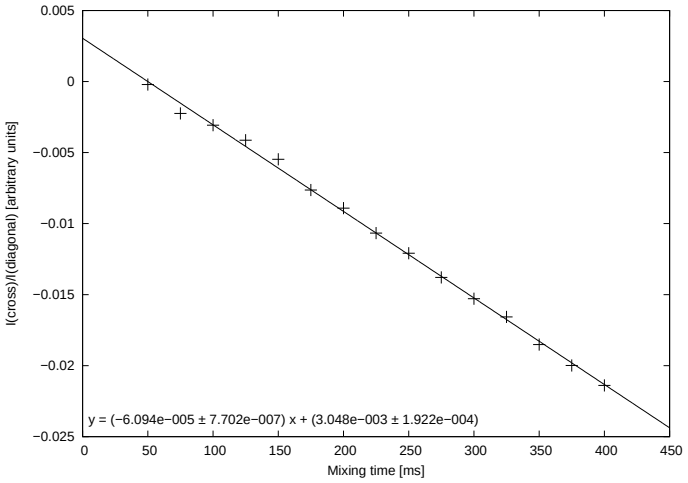

(ae) H_{20b}–H_{18b}

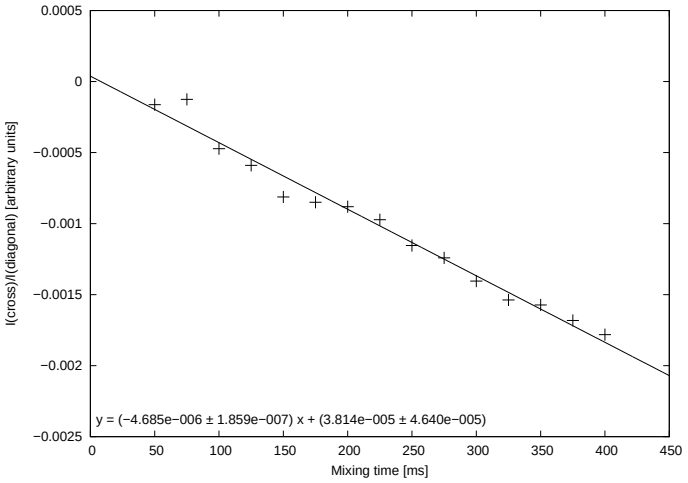

(af) H_{18b}–H_{16}

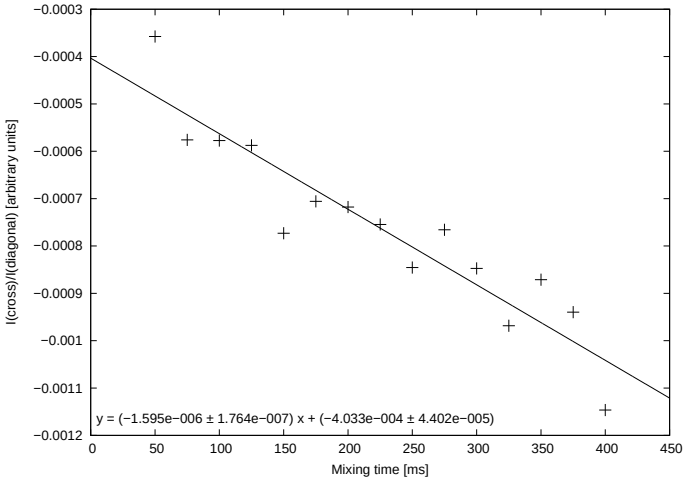

(ag) H_{16}–H_{18b}

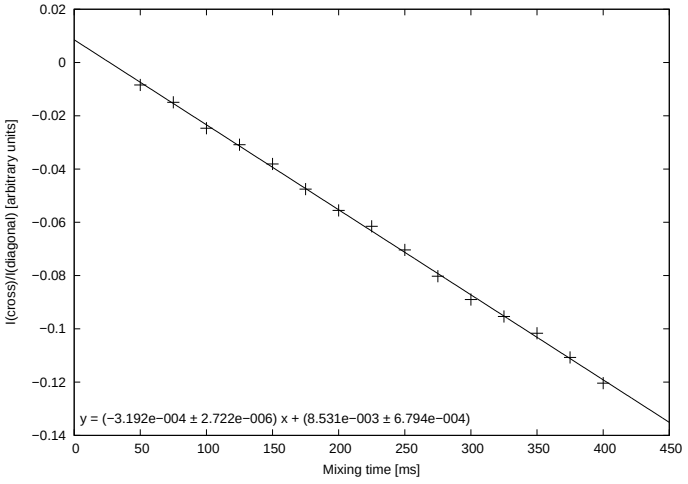

(ah) H_{18b}–H_{18a}

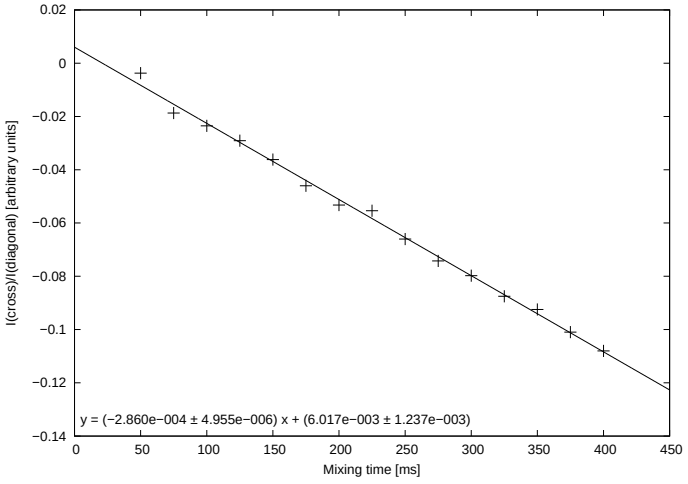

(ai) H_{18a}–H_{18b}

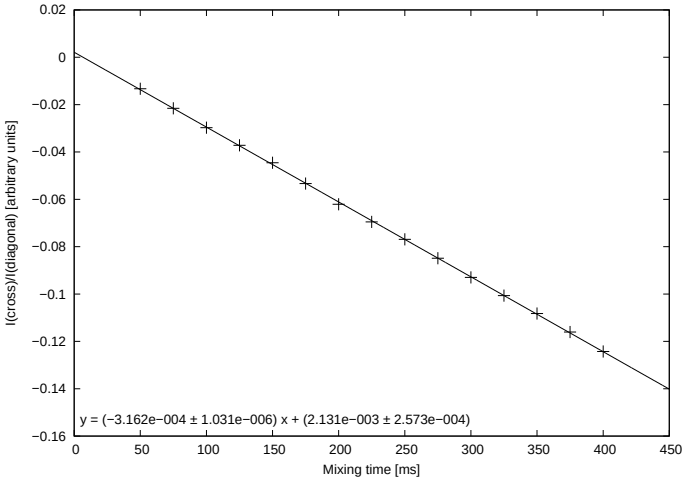

(aj) H_{20b}–H_{20a}

Figure SI.7: The experimental PANIC plots for strychnine **1**.

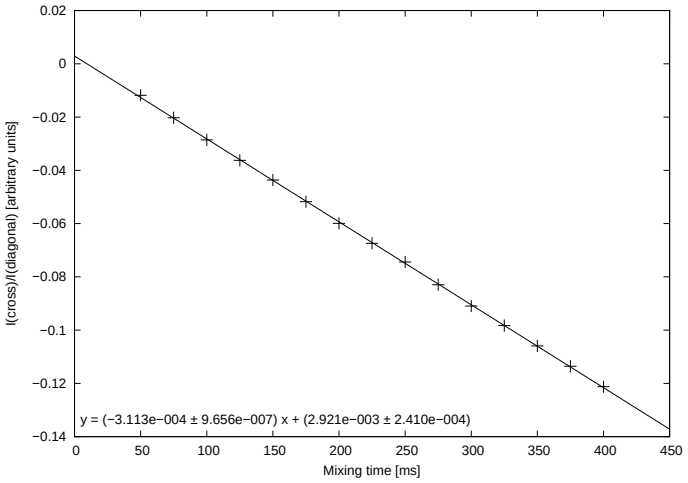

(ak) $H_{20a}-H_{20b}$

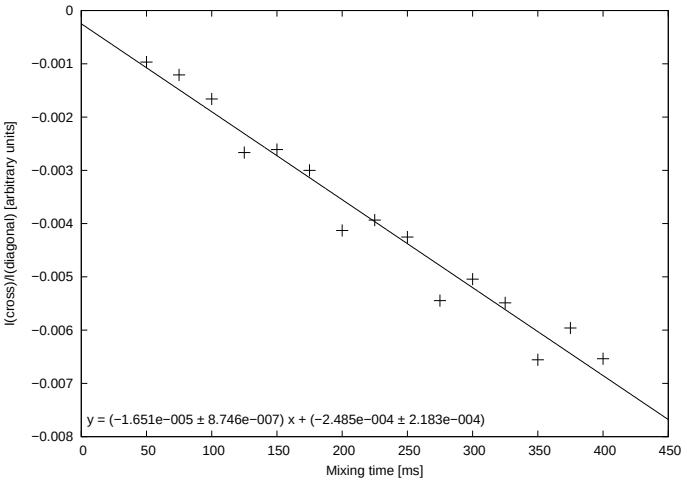

(al) $H_{22}-H_{23a}$

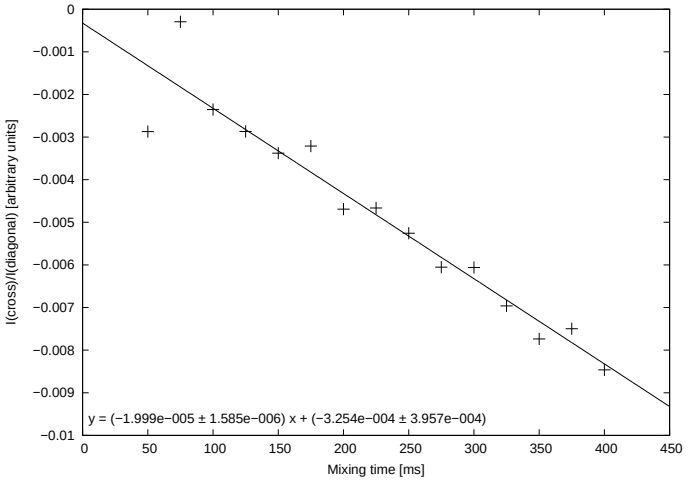

(am) $H_{23a}-H_{22}$

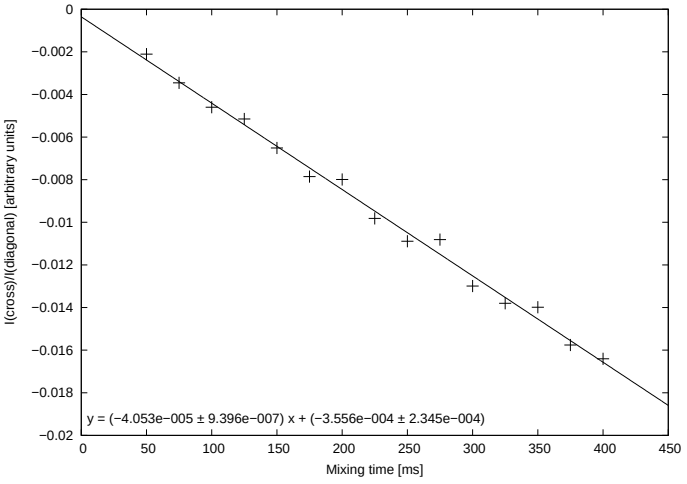

(an) $H_{22}-H_{23b}$

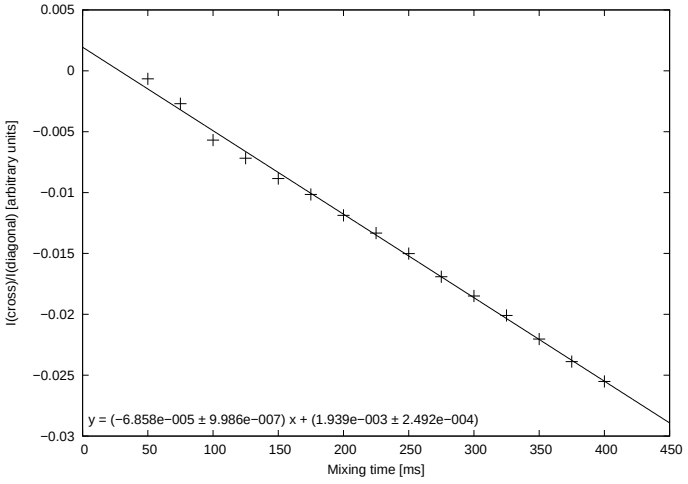

(ao) $H_{23b}-H_{22}$

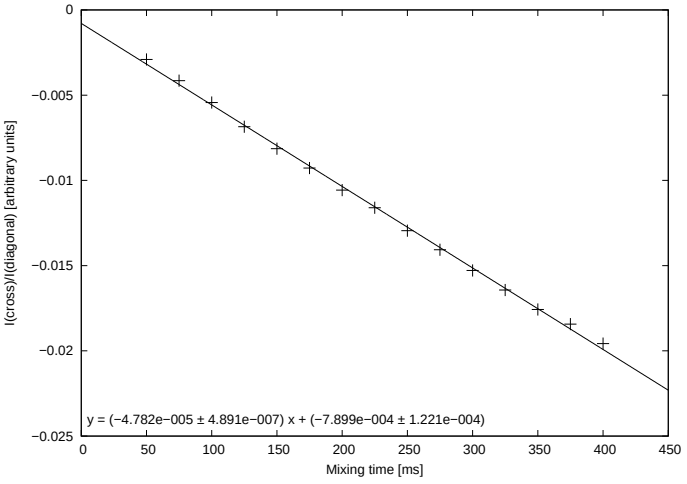

(ap) $H_{22}-H_{20b}$

Figure SI.7: The experimental PANIC plots for strychnine **1**.

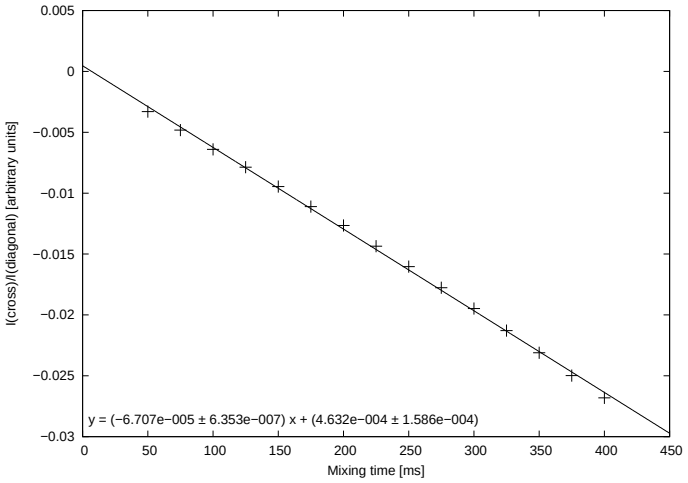

(aq) H_{20b}−H_{22}

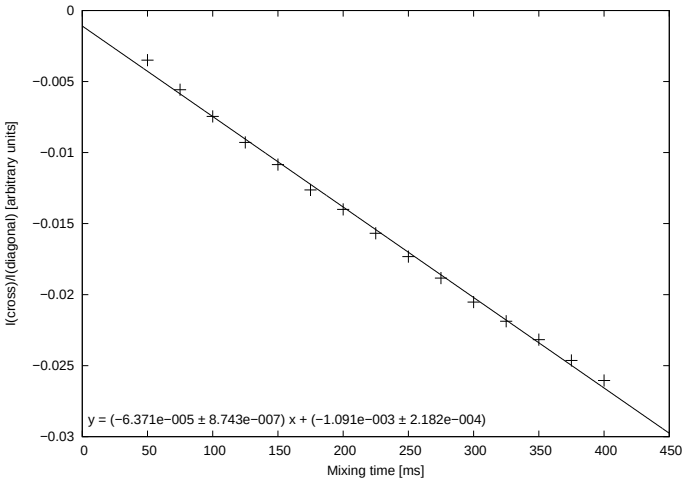

(ar) H_{8}−H_{18b}

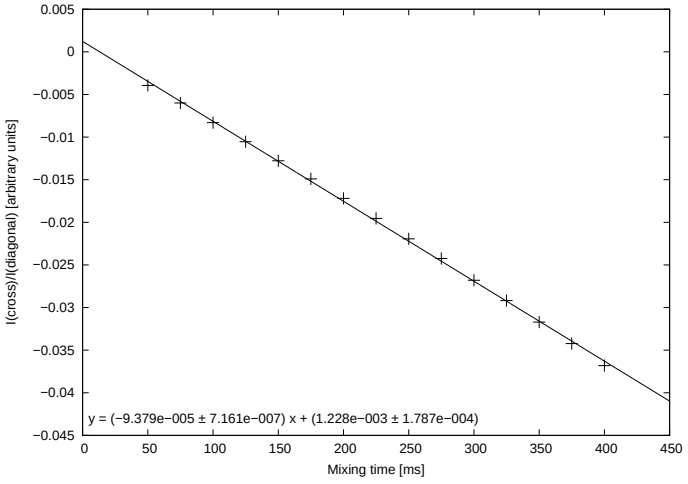

(as) H_{18b}−H_{8}

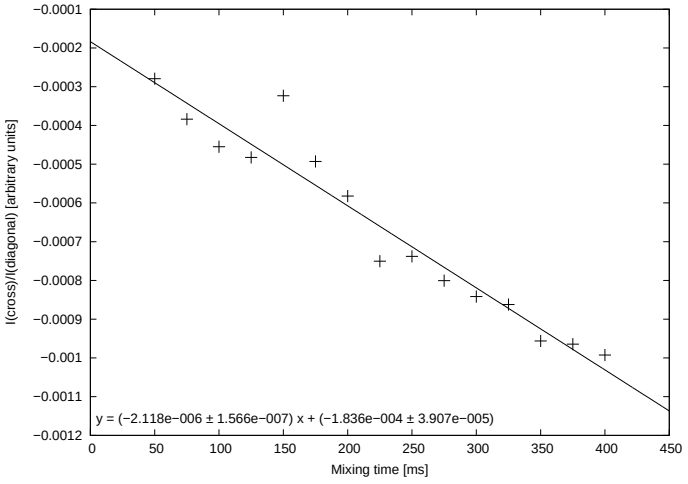

(at) H_{11b}−H_{23a}

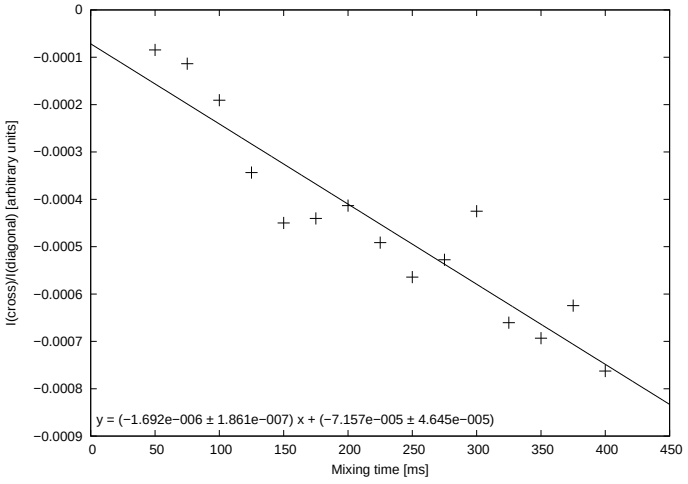

(au) H_{23a}−H_{11b}

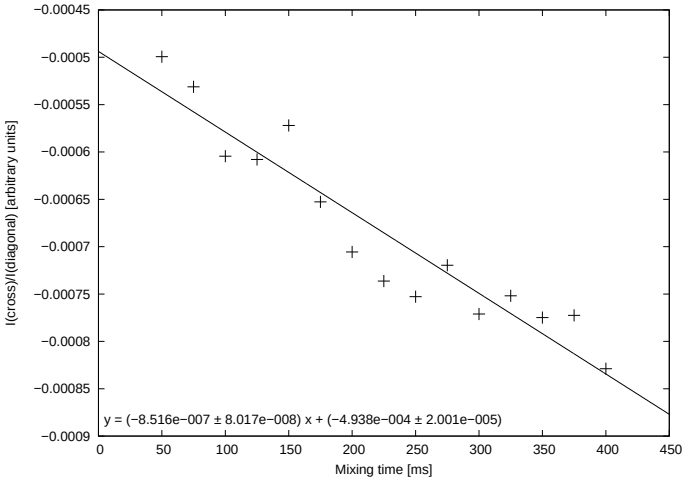

(av) H_{20b}−H_{23b}

Figure SI.7: The experimental PANIC plots for strychnine **1**.

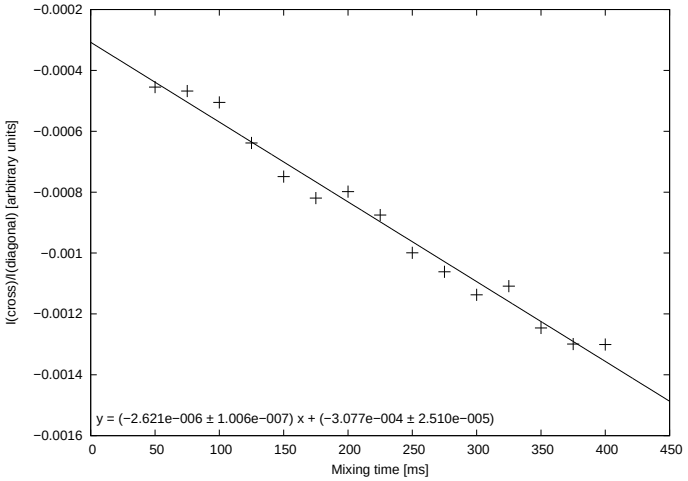

(aw) $H_{20b}-H_{16}$

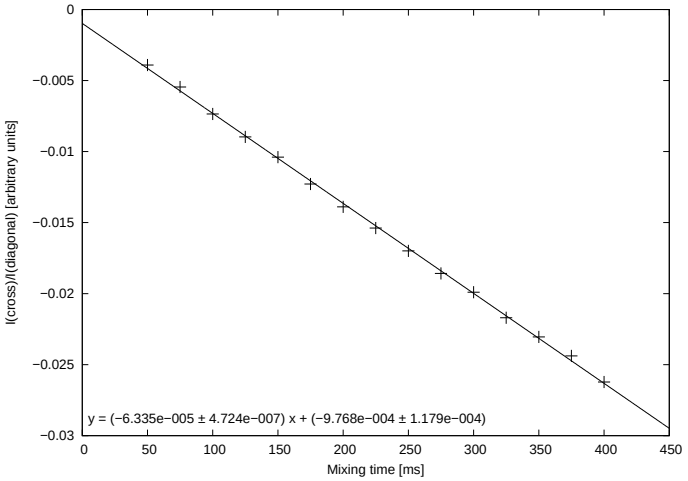

(ax) $H_{12}-H_{23a}$

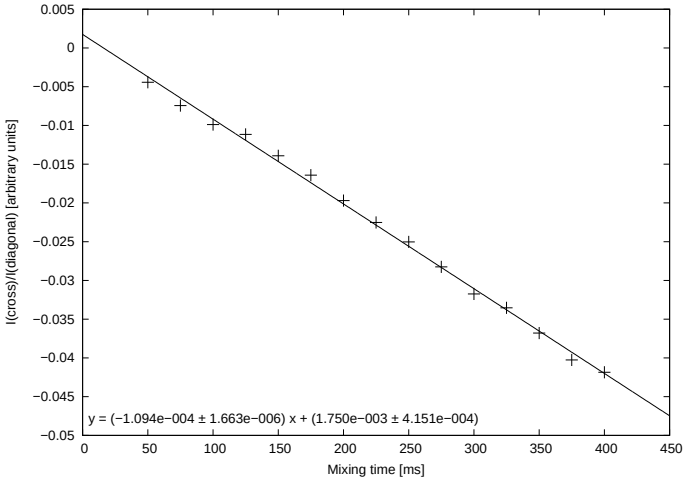

(ay) $H_{23a}-H_{12}$

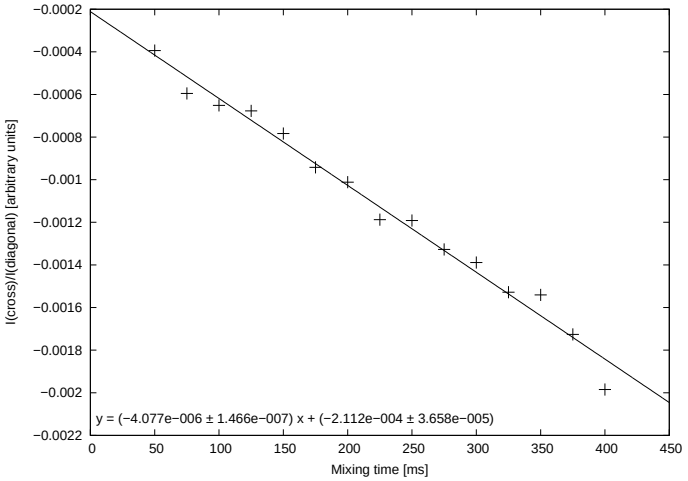

(az) $H_{12}-H_{8}$

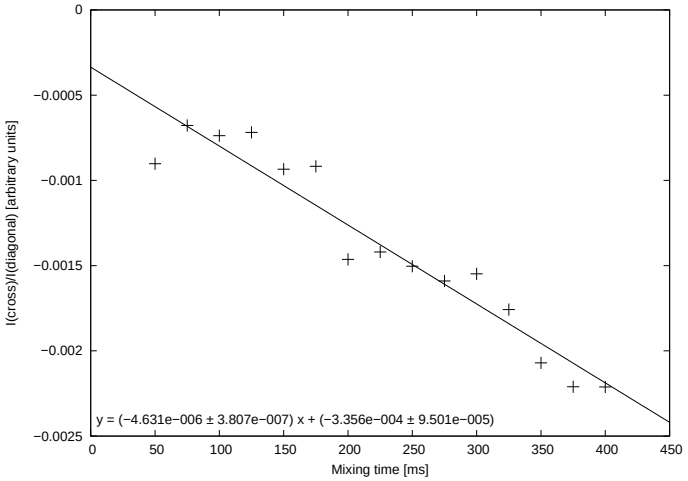

(ba) $H_{8}-H_{12}$

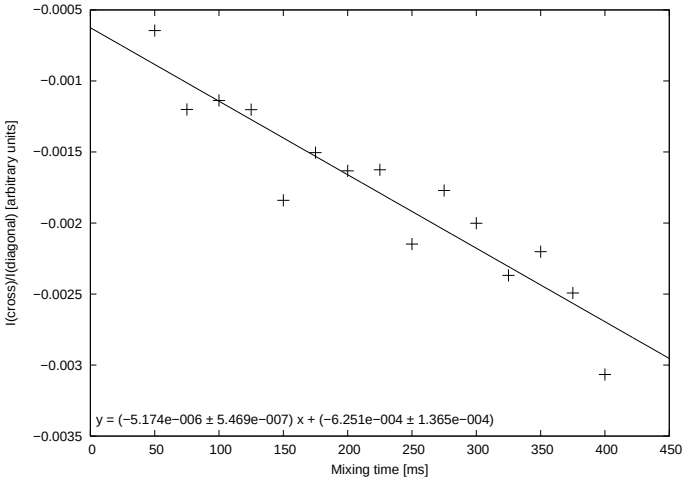

(bb) $H_{16}-H_{20a}$

Figure SI.7: The experimental PANIC plots for strychnine **1**.

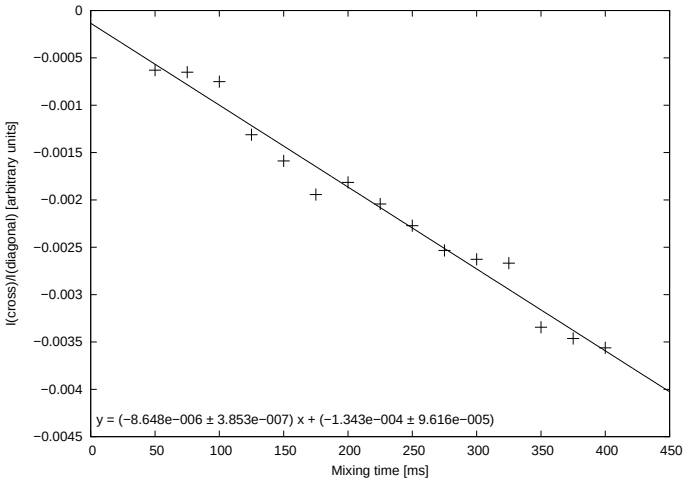

(bc) $H_{20a}-H_{16}$

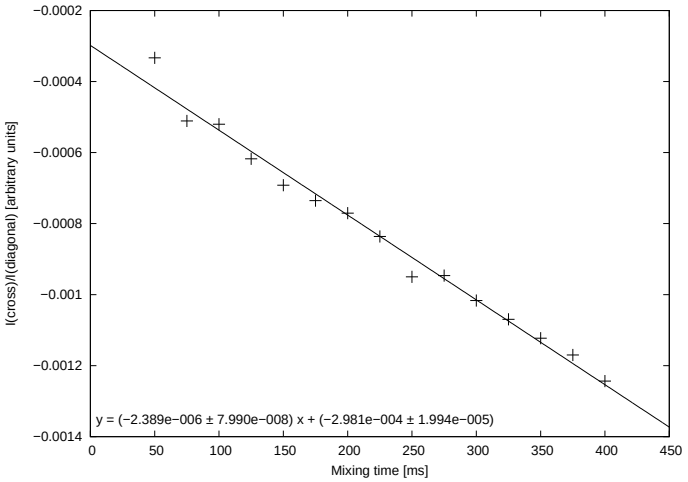

(bd) $H_{16}-H_{13}$

Figure SI.7: The experimental PANIC plots for strychnine **1**.

8. PANIC plots for α-methylene-γ-butyrolactone 2

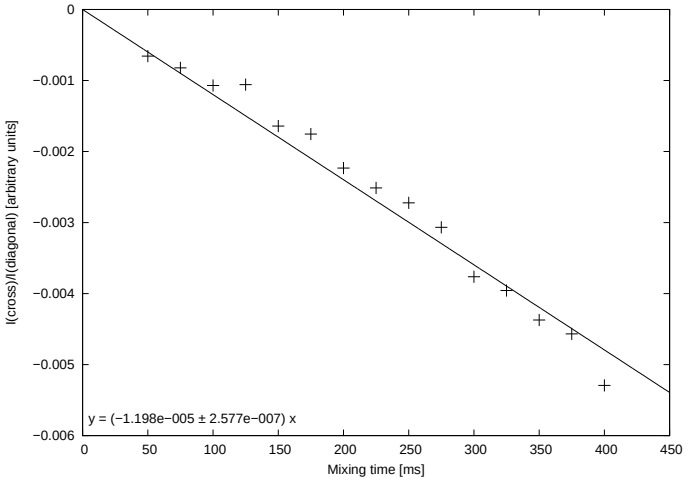

(a) H_1-H_2

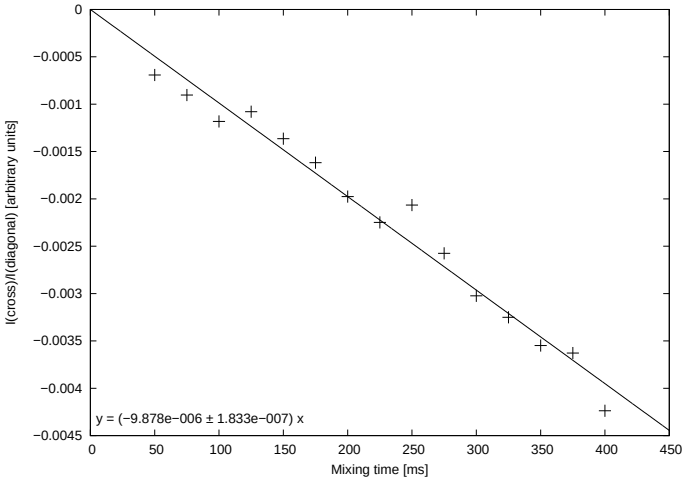

(b) H_1-H_3

Figure SI.8: The PANIC plots for α-methylene-γ-butyrolactone **2**.

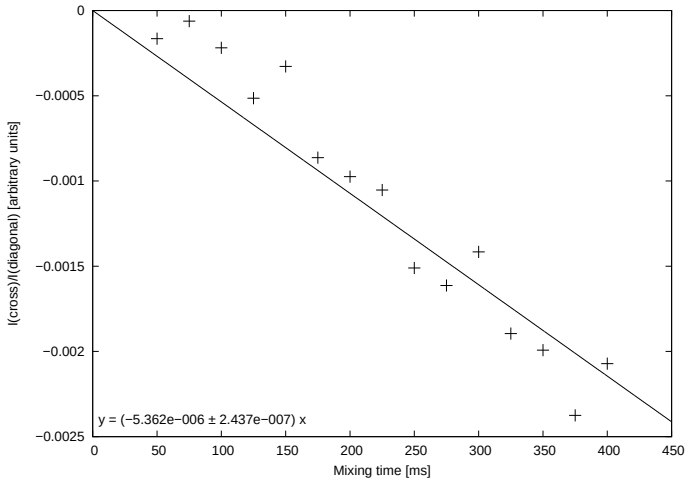

(c) H_2-H_3

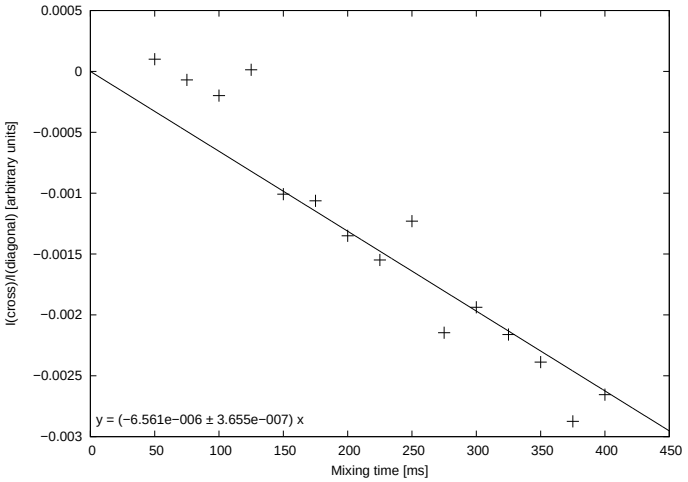

(d) H_3-H_2

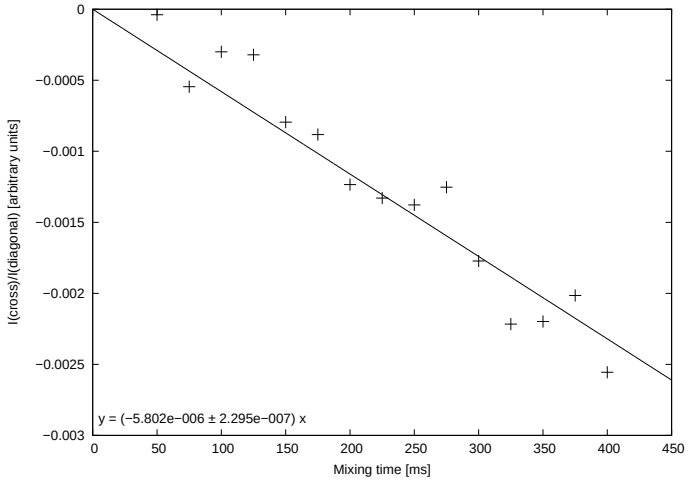

(e) H_3-H_{6b}

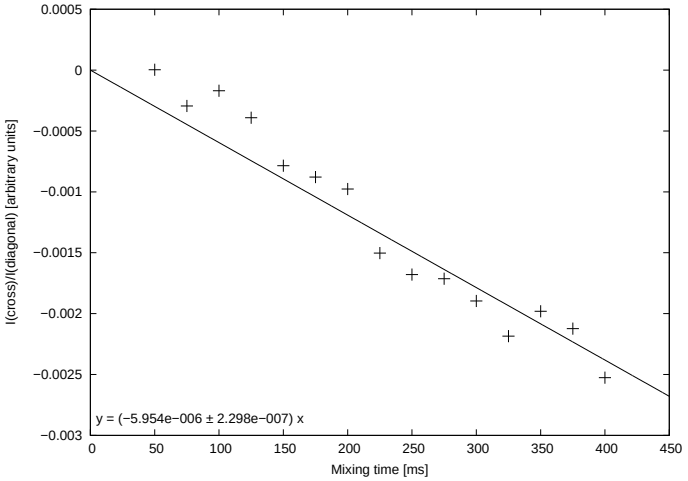

(f) $H_{6b}-H_3$

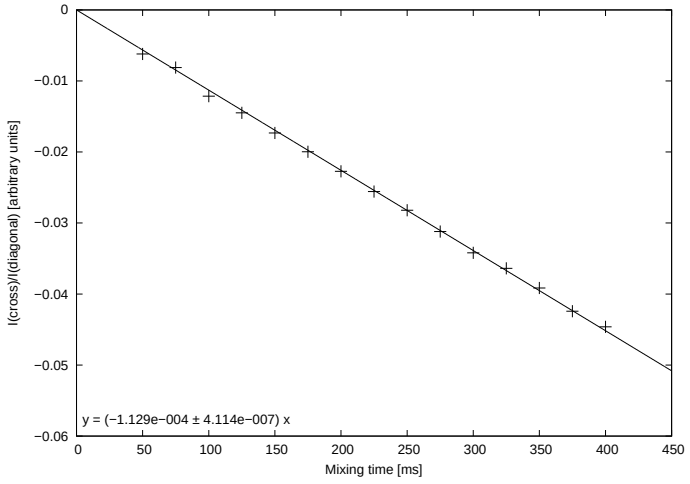

(g) $H_{6a}-H_{6b}$ (used as reference distance)

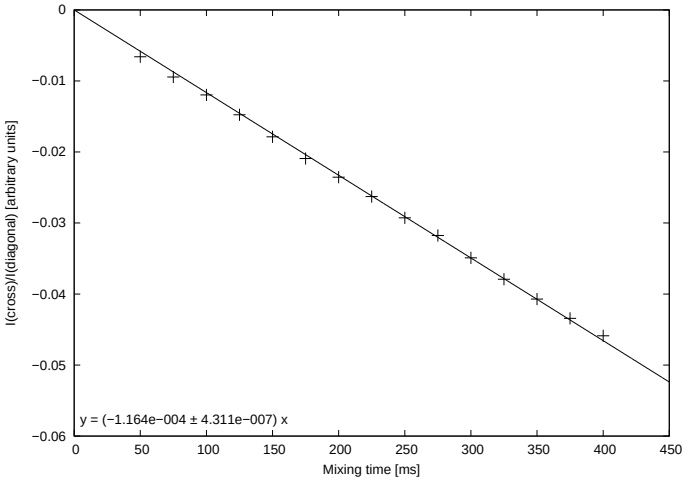

(h) $H_{6b}-H_{6a}$

Figure SI.8: The PANIC plots for α-methylene-γ-butyrolactone **2**.

9. Three-conformer-RDC-fits for strychnine 1

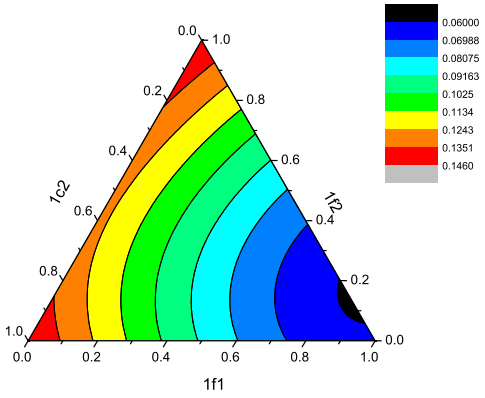

(i) Thiele et al.[10] (no RDCs for C_{23}−H_{23a} and C_{23}−H_{23b}, no RDCs for ring C)

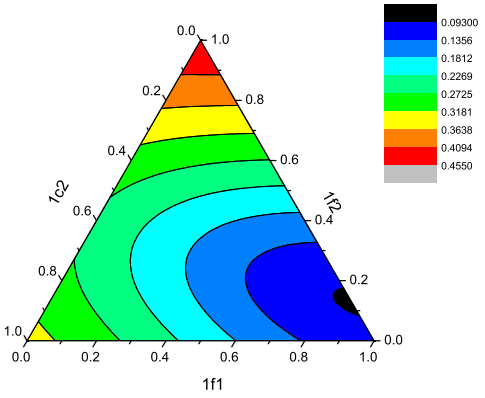

(j) Thiele[11] (RDCs for C_{23}−H_{23a} and C_{23}−H_{23b}, RDCs for ring C)

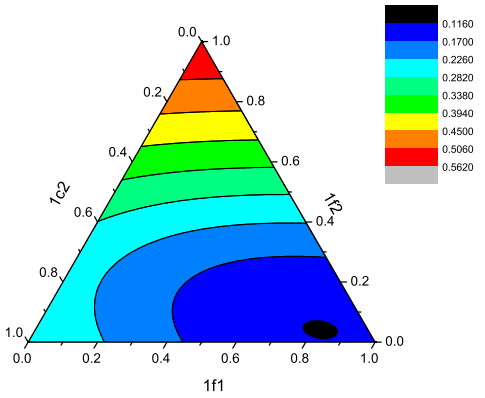

(k) Luy et al.[12](RDCs for C_{23}−H_{23a} and C_{23}−H_{23b}, RDCs for ring C)

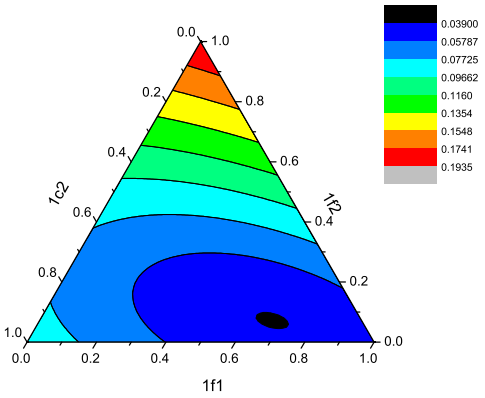

(l) Meyer et al. 1[13](no RDCs for C_{23}−H_{23a} and C_{23}−H_{23b}, no RDCs for ring C)

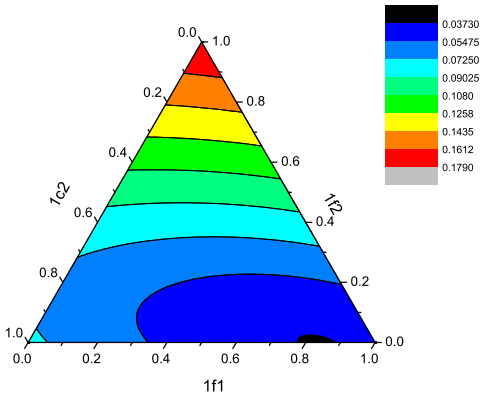

(m) Meyer et al. 2[13](no RDCs for C_{23}−H_{23a} and C_{23}−H_{23b}, no RDCs for ring C)

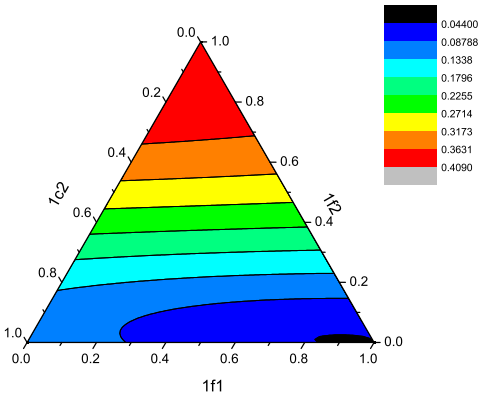

(n) Meyer[14](RDCs for C_{23}−H_{23a} and C_{23}−H_{23b}, no RDCs for ring C)

Figure SI.9: Three-conformer-RDC-fits for strychnine **1**.

10. Spinach

The spin dynamics simulation toolbox *Spinach* was used for the spectral simulations in this paper. In this section, details of these simulations are presented.

10.1. Spin system parameters

The ^1H chemical shifts and J_{HH} coupling constants as reported in tables SI.3 and SI.4 were used as input for *Spinach*[15].

We started with the shifts and coupling values as reported in the literature[16,17]. Next, we refined these values by simulation with *Bruker NMR-Sim 5.4* and comparison with a ^1H spectrum recorded at our 600 MHz spectrometer as described in section 1 (see figure SI.10). The simulated and experimental spectra are in very good agreement, except for H_{18a} and $H_{17a/b}$. Those protons are not important for our simulations, thus we chose to ignore this discrepancy. It should be noted that the signals of H_{14} and H_{11a} overlap in the experimental spectrum. In the simulated spectra, those two protons were refined individually.

Relaxation was included using a Bloch–Wangsness–Redfield superoperator[18] with isotropic rotational correlation time 200 ps.

The IK–2(2) basis set[15] was used for each conformer. This basis was determined to be large enough for us to be able to discount spin diffusion effects for the H_{11b}−H_{23b} PANIC plot. This determination was performed by comparing the individual conformer plots with those generated using the IK–2(4) basis; this latter basis is equivalent to that found in Reference[19] to capture spin diffusion effects. This comparison is shown in table SI.5. The agreement of the data of the PANIC plots for the two basis sets is perfect. The bases of the two exchanging systems were taken to be the union of the bases required for each system in order that the bases be closed with respect to exchange. The distance cut-off was taken to be 6 Å; this distance was chosen to be larger than any of the distances of interest in the conformers.

Table SI.3: Proton chemical shifts of strychnine **1** used as input for Spinach. See figure 1 of the main text for nomenclature.

proton	chemical shift/ppm
H_3	7.1771
H_{22}	5.8527
H_2	7.0211
H_1	7.0924
H_4	8.0149
H_{12}	4.2119
H_{23b}	4.0750
H_{23a}	3.9913
H_{16}	3.9094
H_8	3.7905
H_{20b}	2.6864
H_{20a}	3.6556
H_{18a}	3.1692
H_{18b}	2.8140
H_{13}	1.2025
H_{17a}	1.8265
H_{17b}	1.8264
H_{11a}	3.0516
H_{11b}	2.5938
H_{14}	3.0789
H_{15b}	2.2879
H_{15a}	1.3927

Table SI.4: Proton-proton coupling constants of strychnine **1** used as input for Spinach. See figure 1 of the main text for nomenclature.

proton 1	proton 2	J_{HH}/Hz
H_{22}	H_{23a}	6.04
H_{22}	H_{23b}	6.95
H_{14}	H_{22}	0.47
H_{14}	H_{20a}	1.61
H_{23a}	H_{23b}	-13.80
H_{20a}	H_{20b}	-14.80
H_{20a}	H_{22}	1.79
H_{23a}	H_{20a}	1.30
H_{14}	H_{22}	0.47
H_{14}	H_{20a}	1.61
H_{13}	H_{14}	3.29
H_{14}	H_{15a}	1.96
H_{14}	H_{15b}	4.11
H_{17a}	H_{17b}	-13.90
H_{17a}	H_{18a}	5.50
H_{17a}	H_{18b}	7.20
H_{17b}	H_{18a}	3.20
H_{17b}	H_{18b}	10.70
H_{18a}	H_{18b}	-13.90
H_3	H_4	8.05
H_2	H_3	7.44
H_2	H_4	0.98
H_1	H_2	7.49
H_1	H_3	1.08
H_1	H_4	0.23
H_{12}	H_{13}	3.30
H_8	H_{13}	10.41
H_{13}	H_{14}	3.29
H_{11a}	H_{11b}	17.34
H_{11a}	H_{12}	3.34
H_{11b}	H_{12}	8.47
H_{14}	H_{15a}	1.96
H_{14}	H_{15b}	4.11
H_{15a}	H_{15b}	-14.35
H_{15a}	H_{16}	2.42
H_{15b}	H_{16}	4.33

10.2. Pulsed field gradient spin echo element

The experimental pulse sequence utilised a pulsed field gradient spin echo element. This element was simulated using the analytical result found in Reference [3].

10.3. Exchange

The state of the system of conformers is taken to be a direct sum of the states representing the conformers weighted by their respective concentrations. The Liouvillian [20] generating the dynamics of the individual systems is then block diagonal. Inclusion of an additional exchange superoperator consisting of diagonal blocks weighted by the appropriate exchange rates gives exchange between the systems. Exchange rates are chosen so as to maintain the relative proportions of the conformers in equilibrium.

10.4. Zero quantum suppression

Zero quantum suppression (ZQS) is effected in the experimental pulse sequence using the Thrippleton–Keeler element [4]. This element consists of a swept frequency π-pulse contemporaneous with a z-axis-field gradient of strength G applied over a time τ_p. This element was simulated in the manner described below.

Following the arguments of Thrippleton and Keeler [4], a molecule at position α (where α runs from 0 to 1) in the sample can be considered to evolve under the propagator

$$\hat{P}_\alpha^{RF} = \mathrm{e}^{-\mathrm{i}\hat{L}\tau_\mathrm{p}(1-\alpha)}\mathrm{e}^{-\mathrm{i}\hat{I}_x\pi}\mathrm{e}^{-\mathrm{i}\hat{L}\tau_\mathrm{p}\alpha}, \qquad \text{(SI.2)}$$

where $\hat{L}$ is the Liouvillian of the system [20], and $\hat{I}_x$ is a sum over all single-spin x-superoperators [20] of the spins in the molecule that are excited by the swept-frequency pulse.

The propagator in Equation SI.2 is defined in the frame rotating at the frequency $\omega_\mathrm{ref} + \alpha\omega_G$, where ω_ref is the rotating frame frequency used in the rest of the simulation, and $\alpha\omega_G$ is an additional frequency due to the presence of the field gradient [21]. Moving the propagator into the rotating frame of the rest of the experiment results in

$$\hat{P}_\alpha = \mathrm{e}^{-\mathrm{i}\omega_G\hat{I}_z\tau_\mathrm{p}\alpha}\hat{P}_\alpha^{RF}, \qquad \text{(SI.3)}$$

where $\hat{I}_z$ is the sum over all single-spin z-superoperators of the spins in the molecule. In the presence of relaxation, exchange, and strong spin–spin couplings we cannot make the further simplifying assumptions found in Reference [4], and so must use the more general propagator of Equation SI.3 to evolve our system.

In order to generate the propagator representing the whole sample, Equation SI.3 must be integrated over α. Following a commonly used method to simulate the effects of gradients in NMR [22,23], this integral is approximated using a Riemann sum:

$$\int_0^1 \hat{P}_\alpha \,\mathrm{d}\alpha \sim \frac{1}{n}\sum_{i=1}^{n}\hat{P}_{i/n}. \qquad \text{(SI.4)}$$

This sum converges to the desired integral for sufficiently large n. The number of slices n used in the simulations was 20: this number was found to be sufficient to give good agreement with experimentally observed PANIC plots between two weakly-coupled spins, and to give qualitative agreement with experimentally observed PANIC plots in the strong coupling case. The terms in Equation SI.4 were computed in parallel to speed up the calculation.

Table SI.5: Simulated PANIC plot data for different basis sets. The data is reported in ppm of arbitrary units.

mixing	**1f1**		**1f2**	
time/ms	IK–2(2)	IK–2(4)	IK–2(2)	IK–2(4)
50	-95	-95	-4717	-4717
75	-142	-142	-7065	-7065
100	-187	-187	-9316	-9316
125	-232	-232	-11680	-11680
150	-277	-277	-14037	-14037
175	-320	-320	-16216	-16216
200	-364	-364	-18627	-18627
225	-407	-407	-20959	-20959
250	-448	-448	-23077	-23077
275	-491	-491	-25570	-25570
300	-531	-531	-27806	-27806
325	-571	-571	-29941	-29941
350	-613	-613	-32471	-32471
375	-649	-649	-34558	-34558
400	-691	-691	-36880	-36880

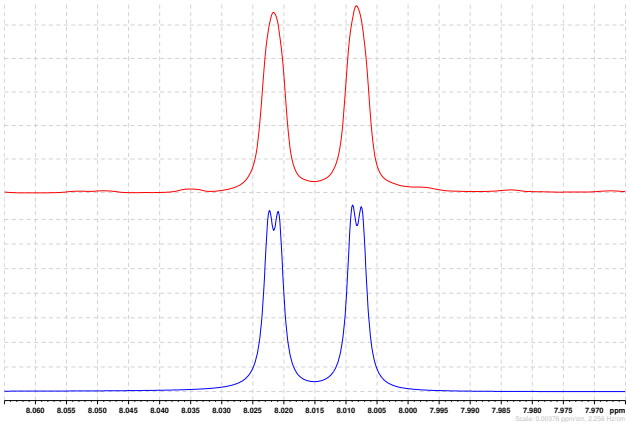

(a) H_4

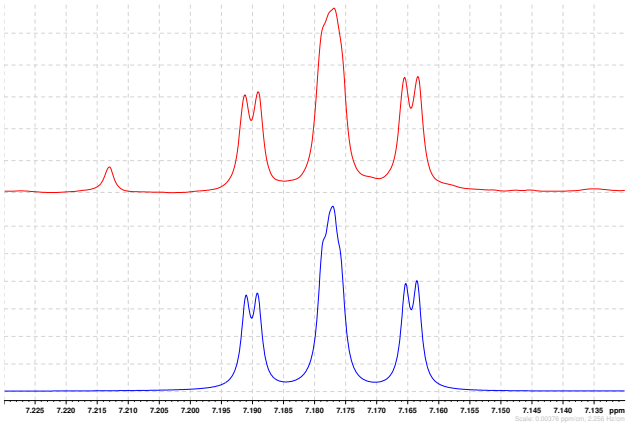

(b) H_3

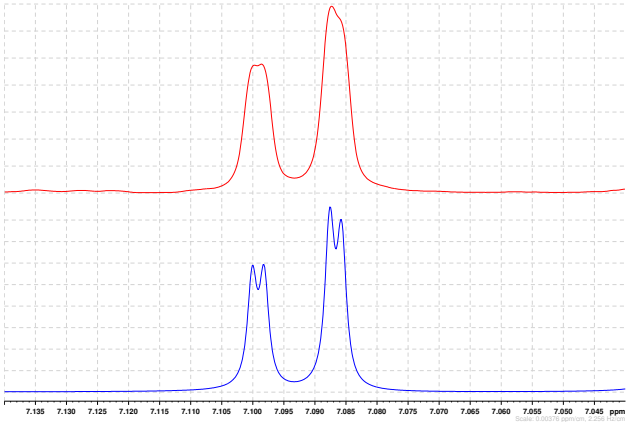

(c) H_1

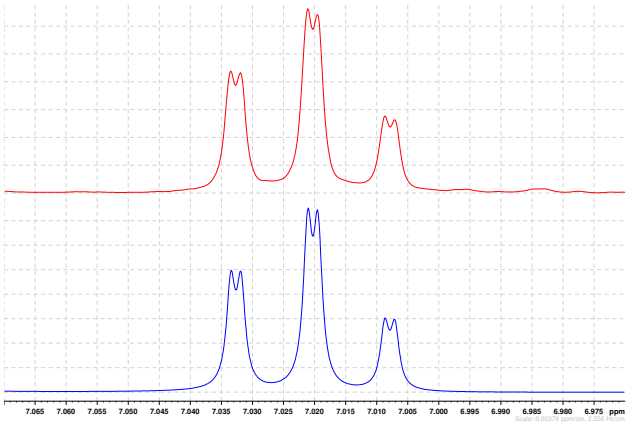

(d) H_2

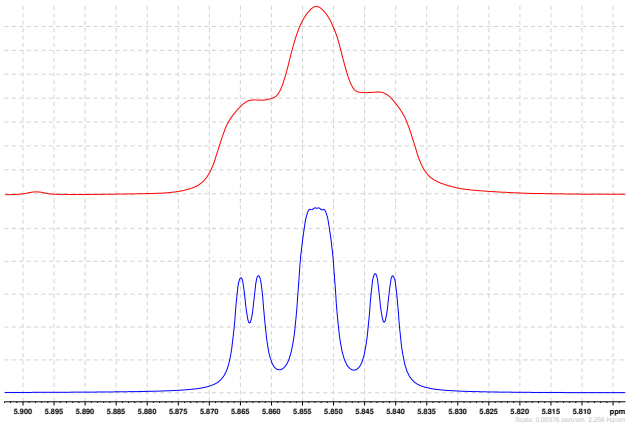

(e) H_{22}

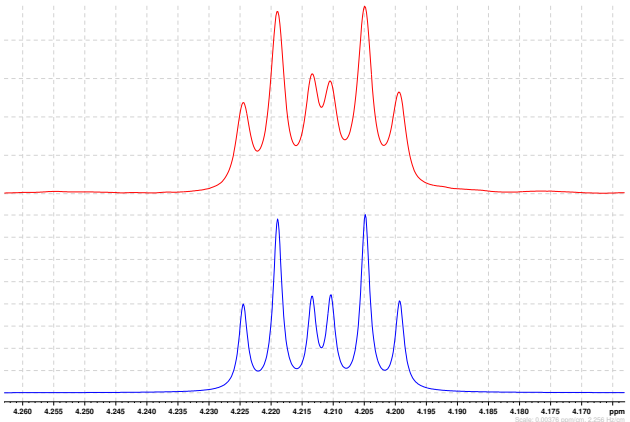

(f) H_{12}

Figure SI.10: Comparison of simulated (*Bruker NMR-Sim 5.4*, bottom, blue) and experimental (600 MHz, top, red) ^1H-spectrum of strychnine **1**.

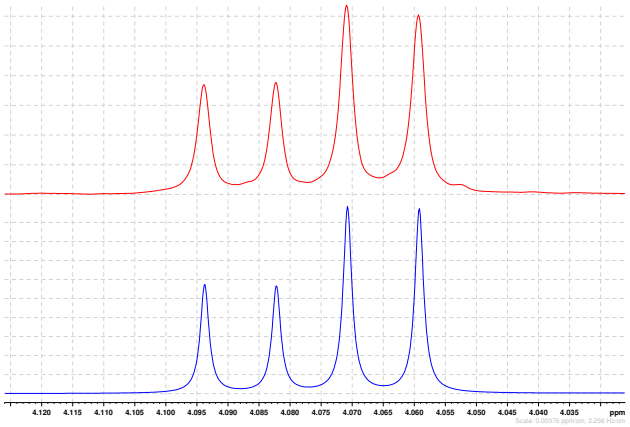

(g) H_{23b}

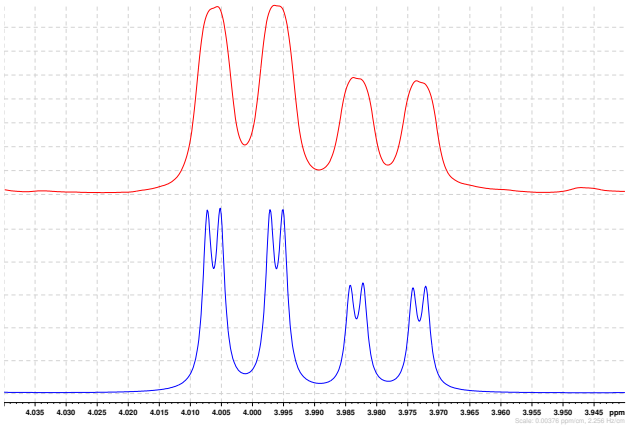

(h) H_{23a}

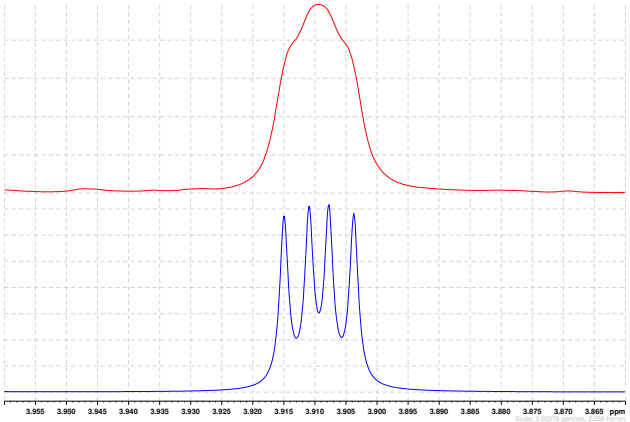

(i) H_{16}

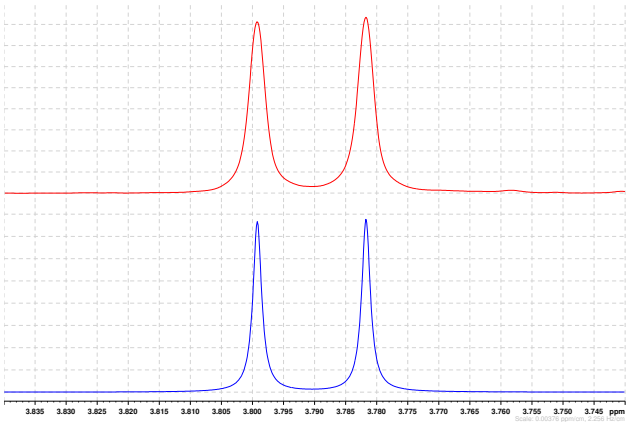

(j) H_8

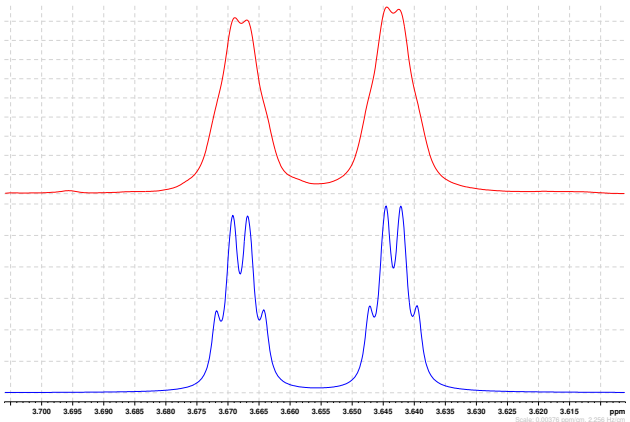

(k) H_{20a}

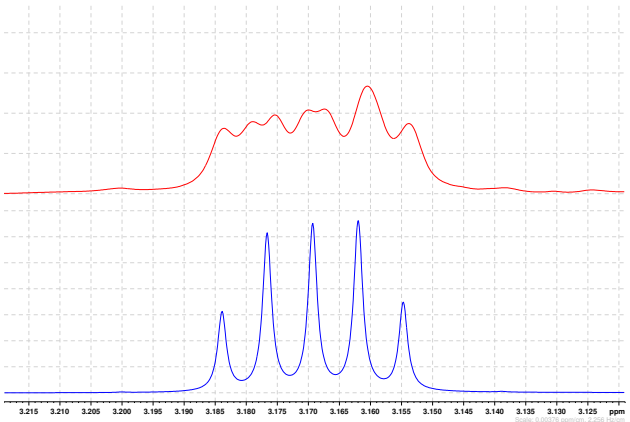

(l) H_{18a}

Figure SI.10: Comparison of simulated (*Bruker NMR-Sim 5.4*, bottom, blue) and experimental (600 MHz, top, red) ^1H-spectrum of strychnine **1**.

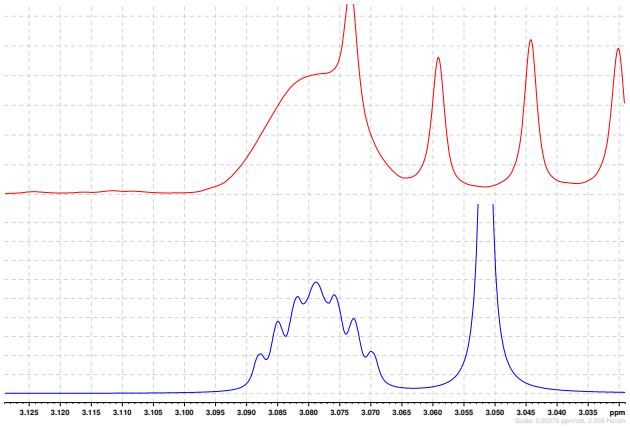

(m) H_{14}

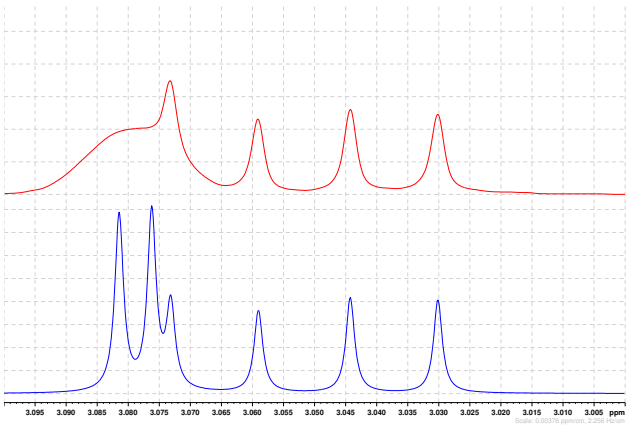

(n) H_{11a}

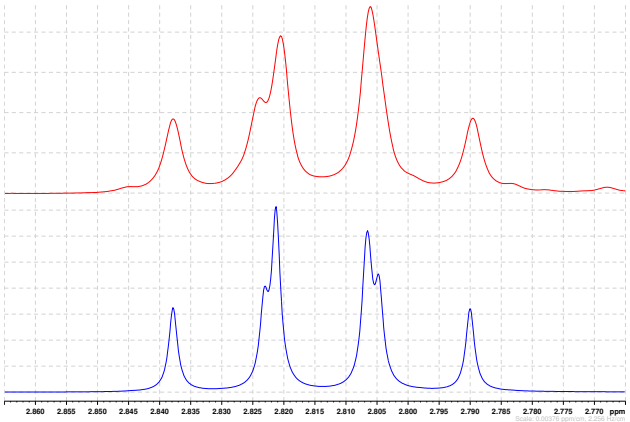

(o) H_{18b}

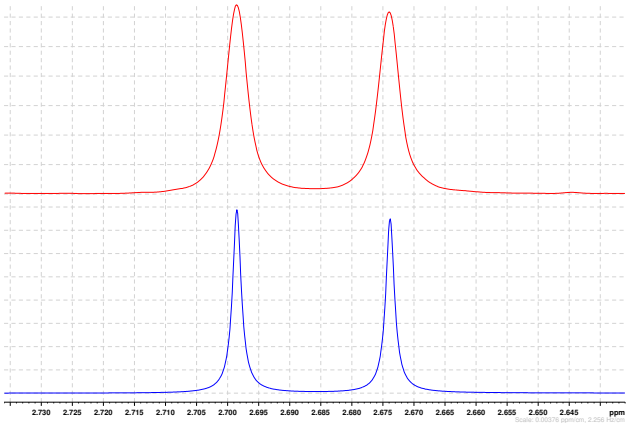

(p) H_{20b}

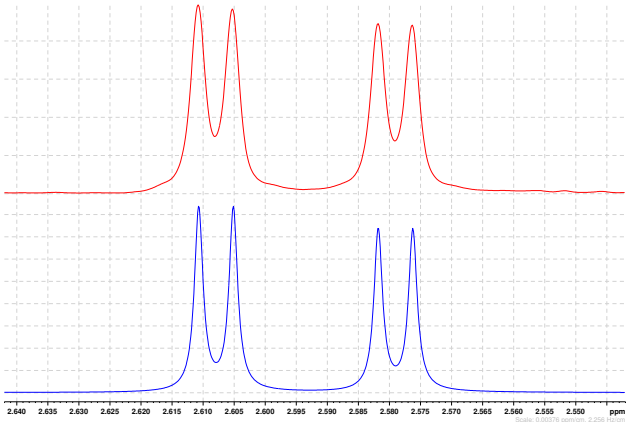

(q) H_{11b}

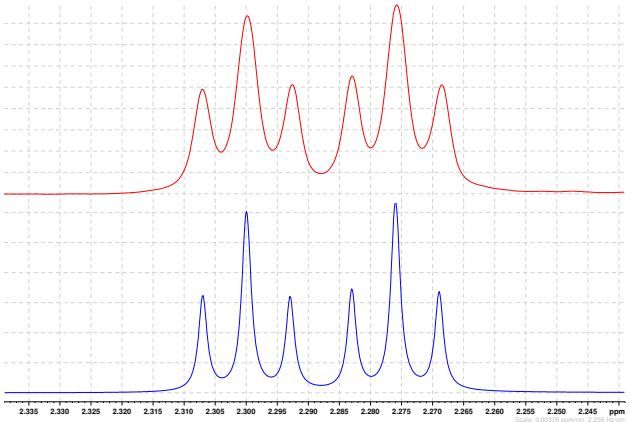

(r) H_{15b}

Figure SI.10: Comparison of simulated (*Bruker NMR-Sim 5.4*, bottom, blue) and experimental (600 MHz, top, red) ^1H-spectrum of strychnine **1**.

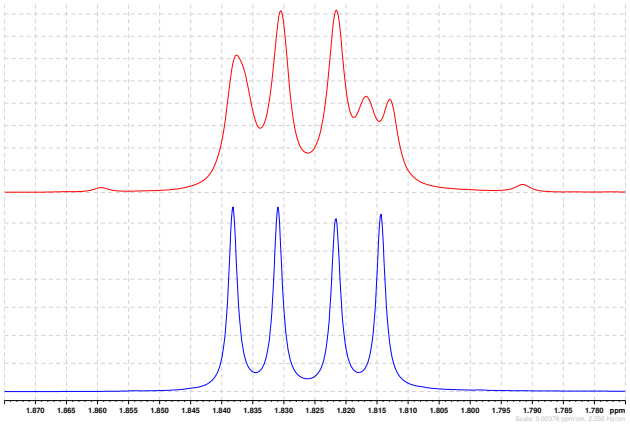

(s) $H_{17a/b}$

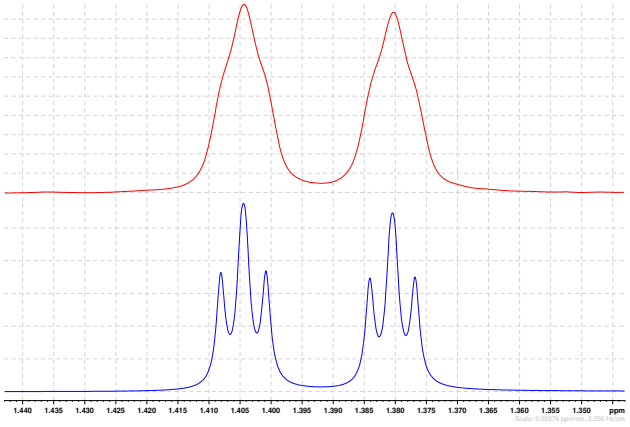

(t) H_{15a}

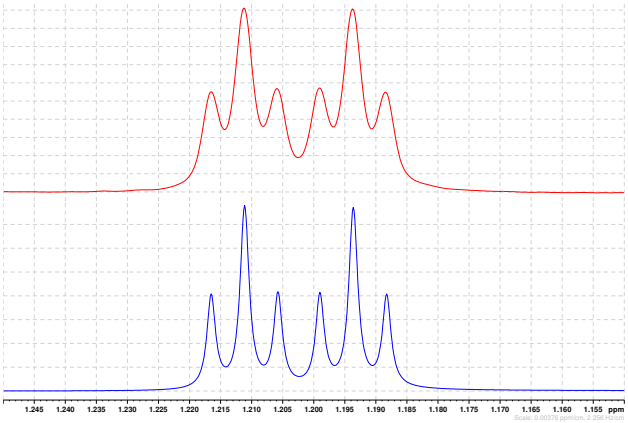

(u) H_{13}

Figure SI.10: Comparison of simulated (*Bruker NMR-Sim 5.4*, bottom, blue) and experimental (600 MHz, top, red) ^1H-spectrum of strychnine **1**.

11. PANIC plots simulated with SPINACH

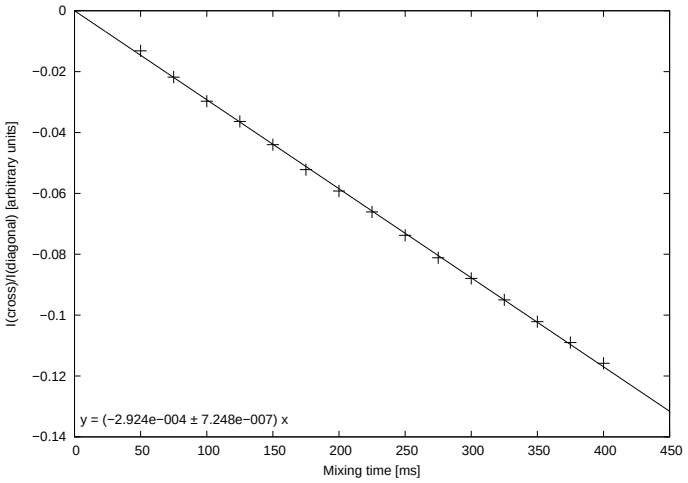

(a) H_{15a}−H_{15b} at 100% **1f1**

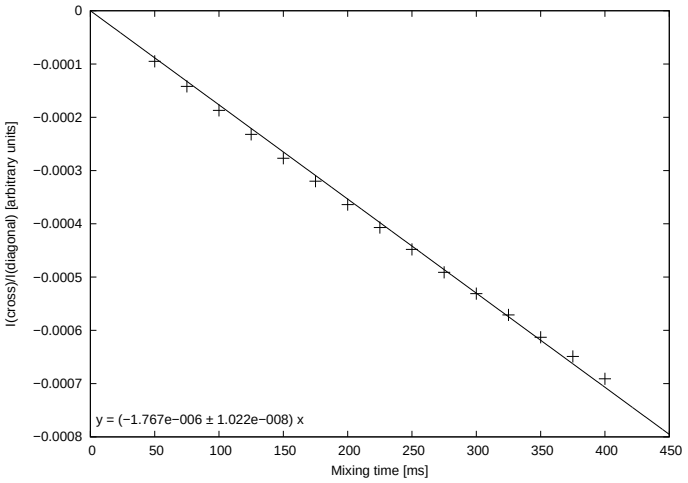

(b) H_{11b}−H_{23b} at 100% **1f1**

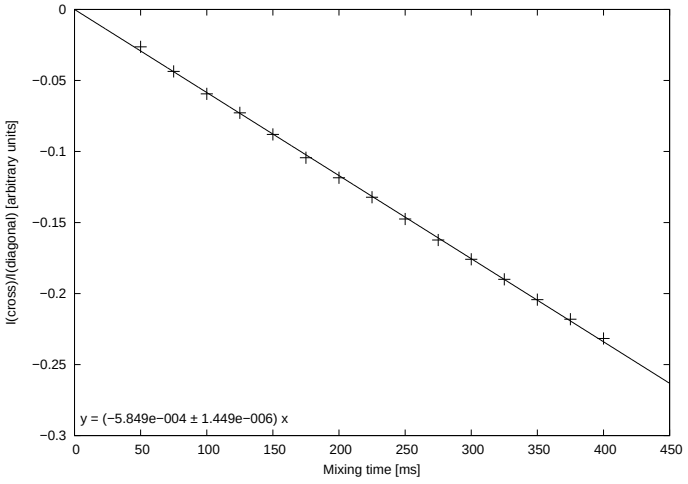

(c) H_{15a}−H_{15b} at 99% **1f1**

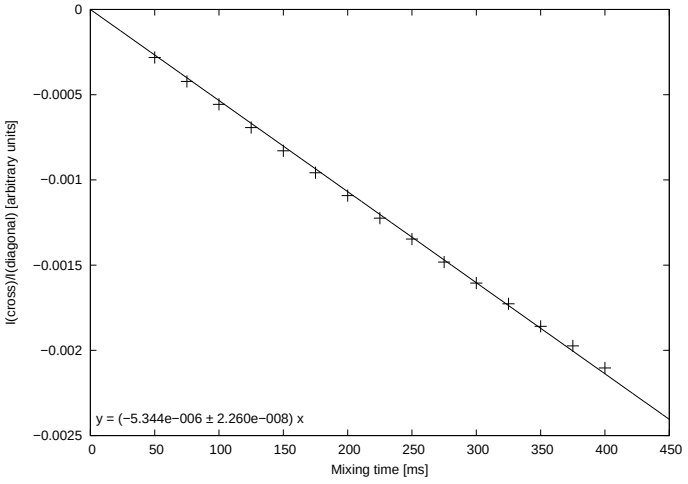

(d) H_{11b}−H_{23b} at 99% **1f1**

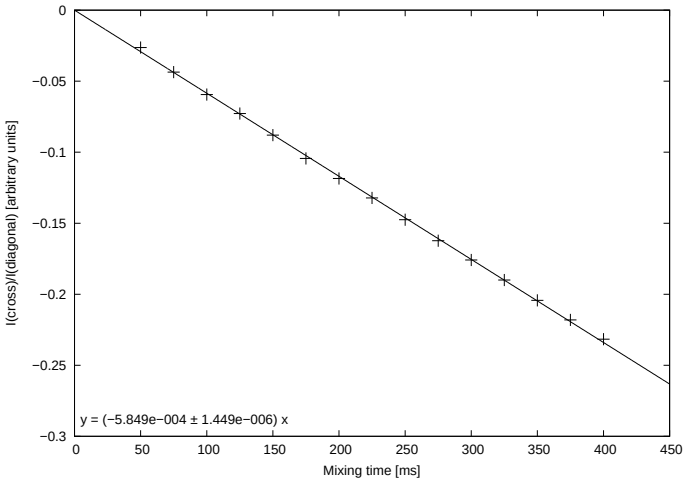

(e) H_{15a}−H_{15b} at 98% **1f1**

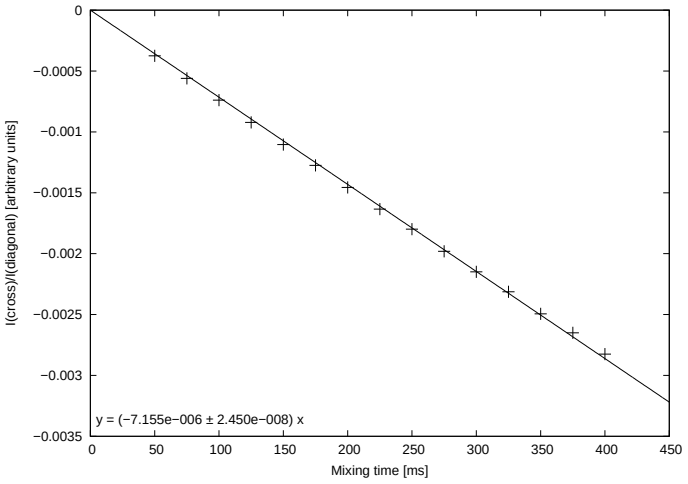

(f) H_{11b}−H_{23b} at 98% **1f1**

Figure SI.11: The simulated PANIC plots for strychnine **1**.

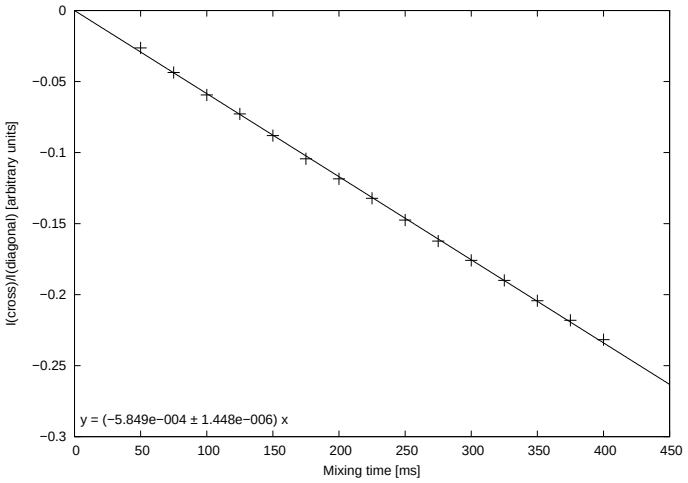

(g) H_{15a}–H_{15b} at 97% **1f1**

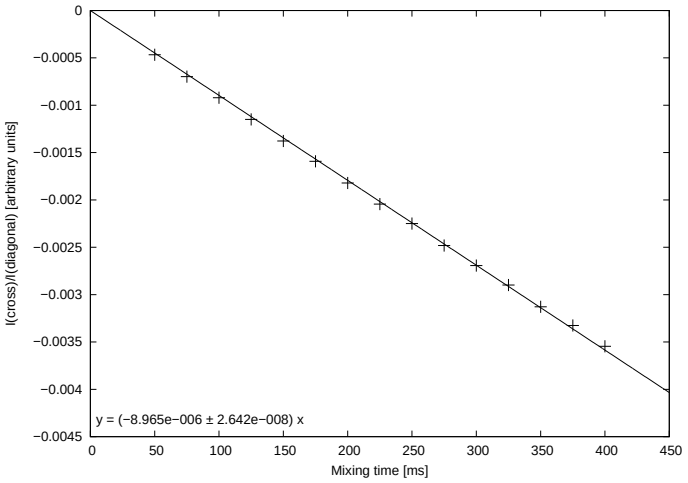

(h) H_{11b}–H_{23b} at 97% **1f1**

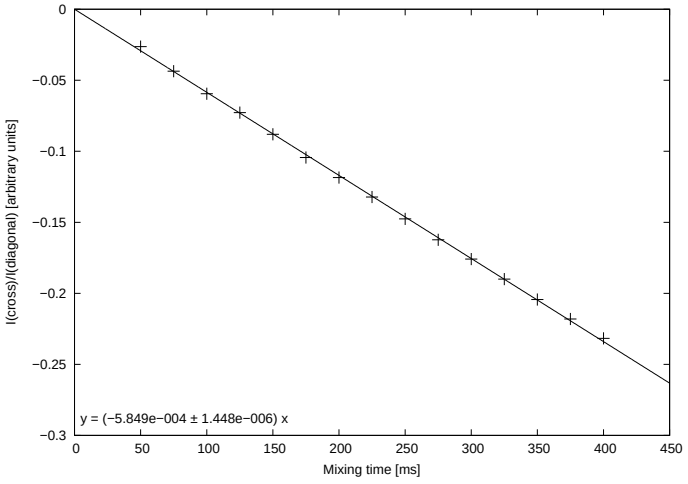

(i) H_{15a}–H_{15b} at 96% **1f1**

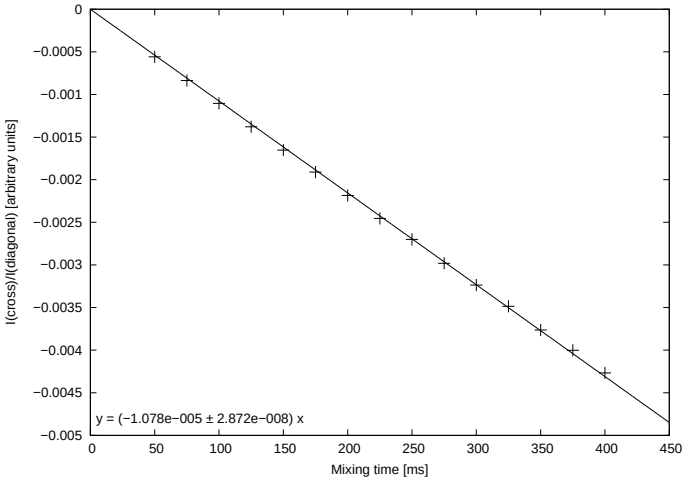

(j) H_{11b}–H_{23b} at 96% **1f1**

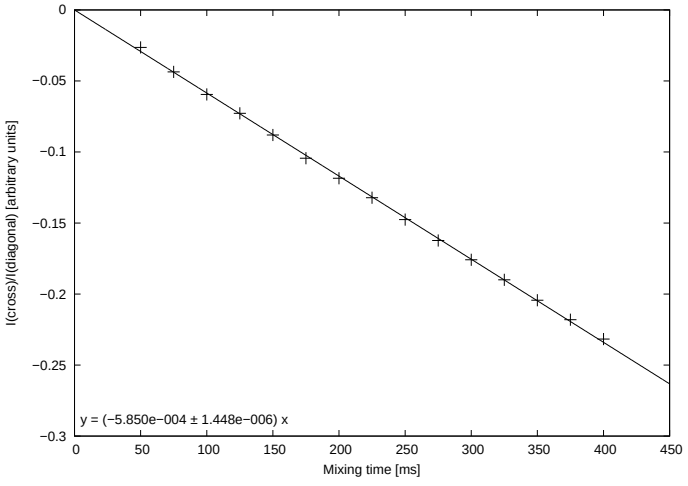

(k) H_{15a}–H_{15b} at 95% **1f1**

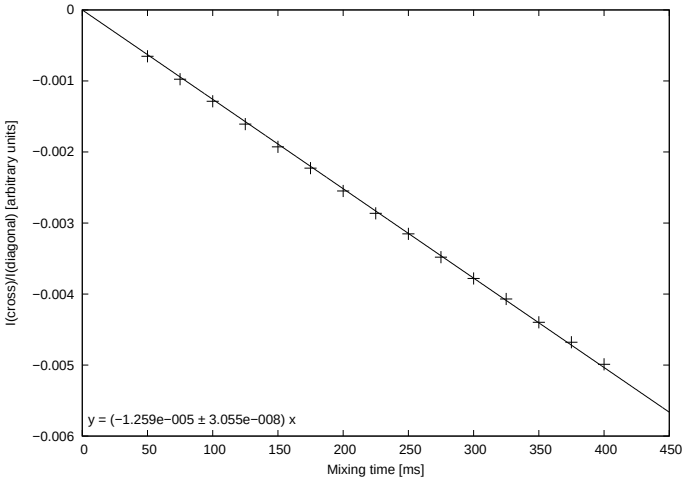

(l) H_{11b}–H_{23b} at 95% **1f1**

Figure SI.11: The simulated PANIC plots for strychnine **1**.

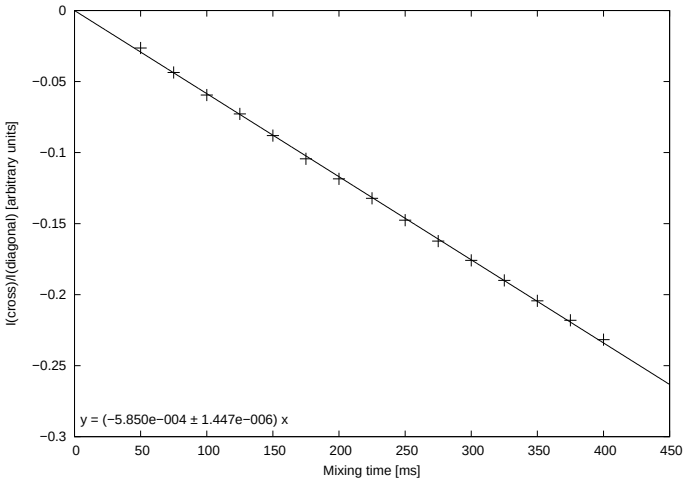

(m) H_{15a}–H_{15b} at 94% **1f1**

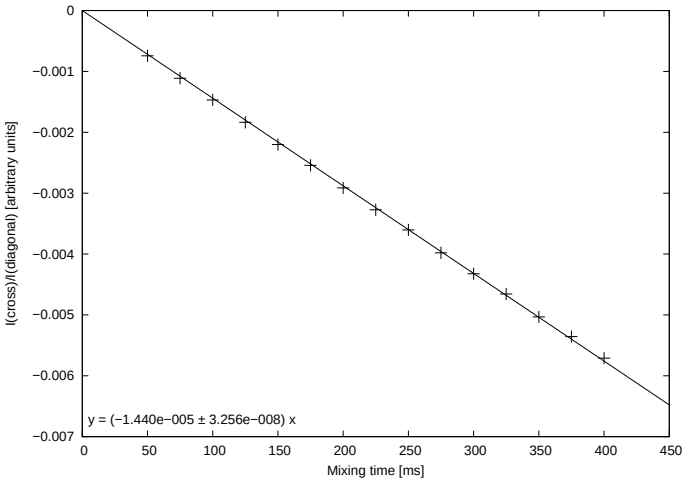

(n) H_{11b}–H_{23b} at 94% **1f1**

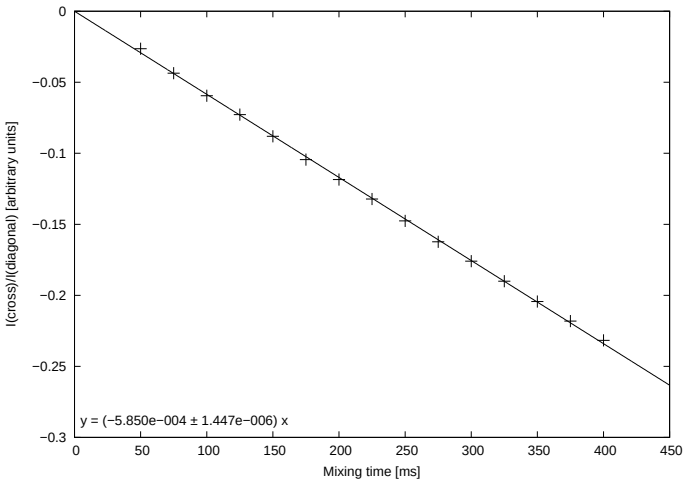

(o) H_{15a}–H_{15b} at 93% **1f1**

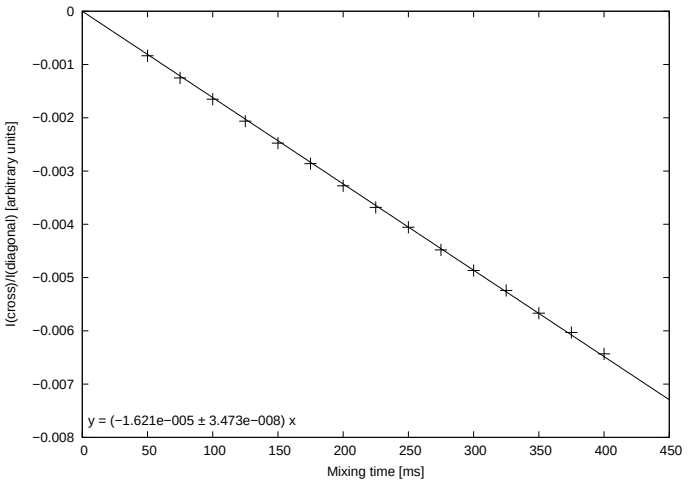

(p) H_{11b}–H_{23b} at 93% **1f1**

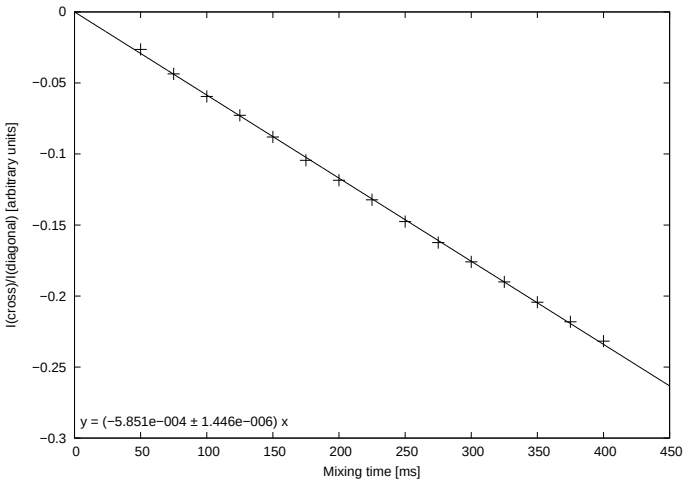

(q) H_{15a}–H_{15b} at 92% **1f1**

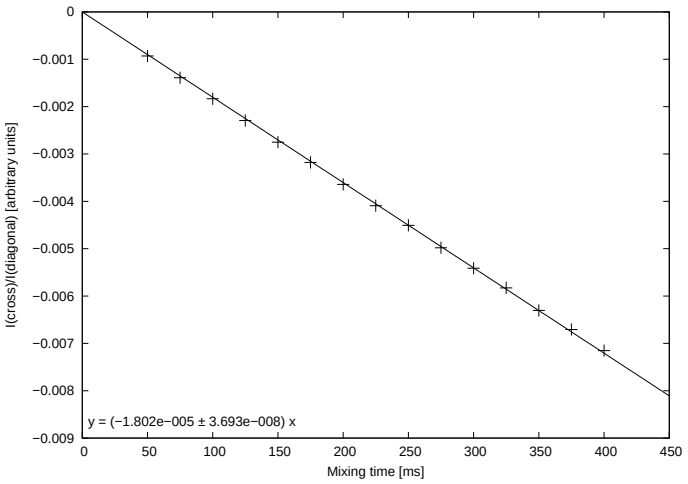

(r) H_{11b}–H_{23b} at 92% **1f1**

Figure SI.11: The simulated PANIC plots for strychnine **1**.

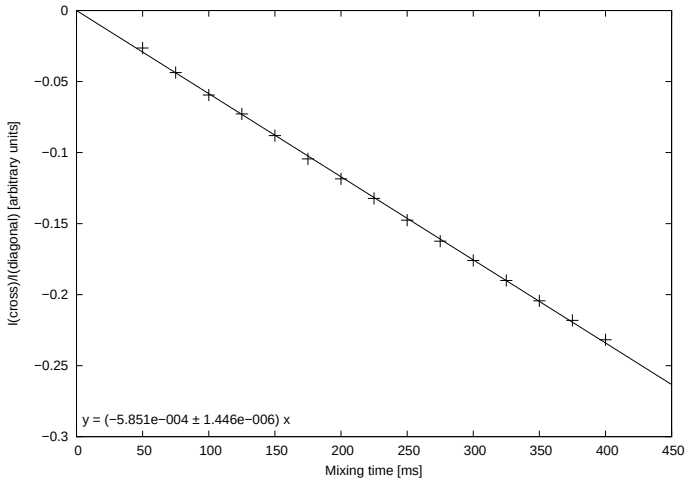

(s) H_{15a}–H_{15b} at 91% **1f1**

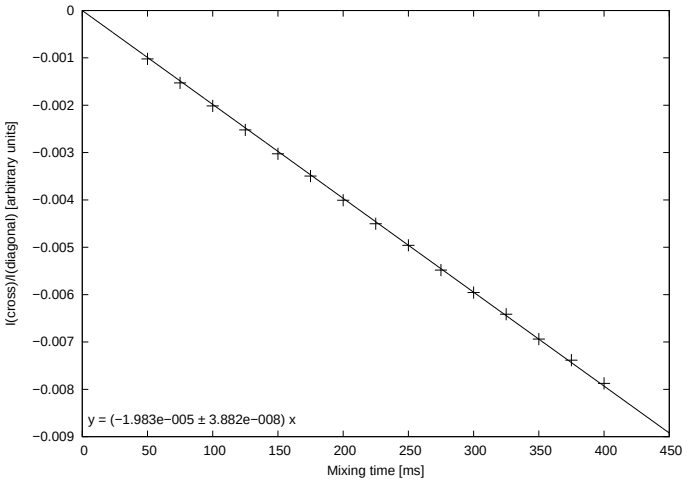

(t) H_{11b}–H_{23b} at 91% **1f1**

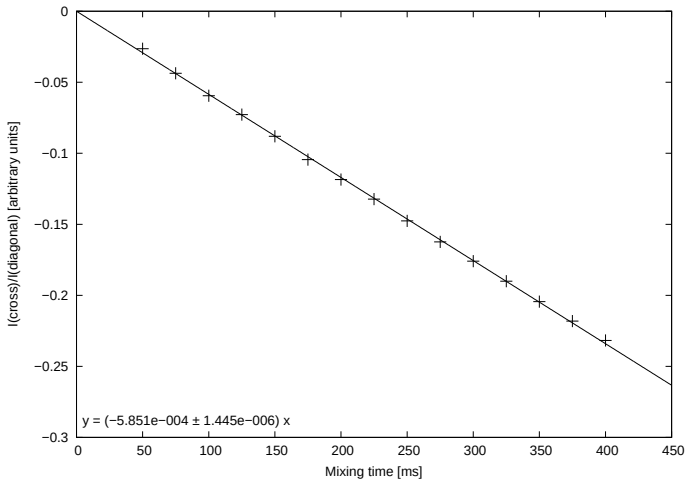

(u) H_{15a}–H_{15b} at 90% **1f1**

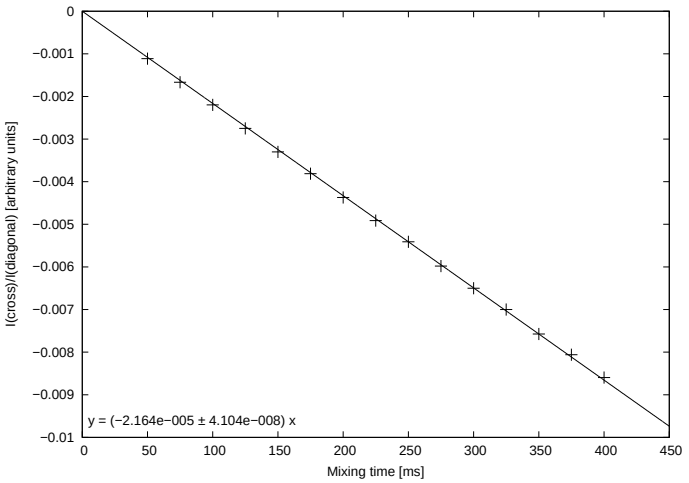

(v) H_{11b}–H_{23b} at 90% **1f1**

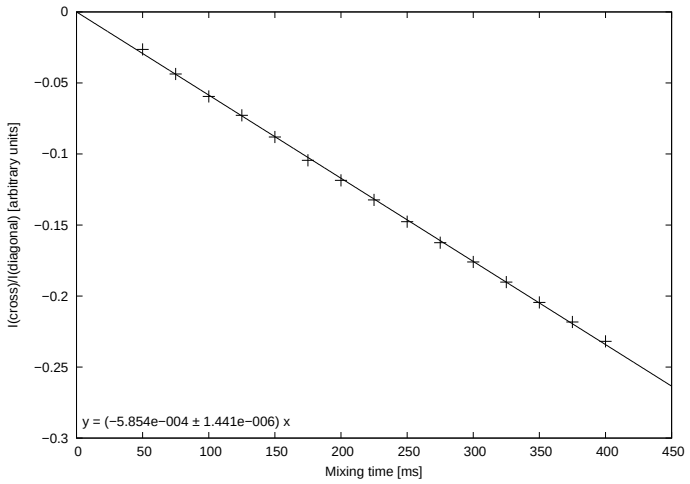

(w) H_{15a}–H_{15b} at 80% **1f1**

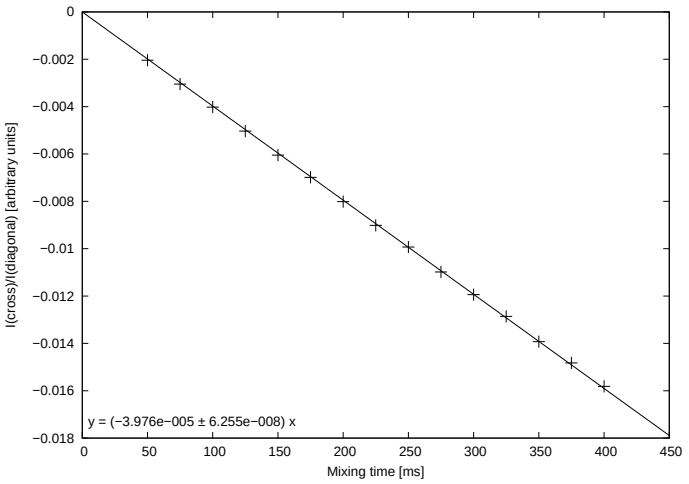

(x) H_{11b}–H_{23b} at 80% **1f1**

Figure SI.11: The simulated PANIC plots for strychnine **1**.

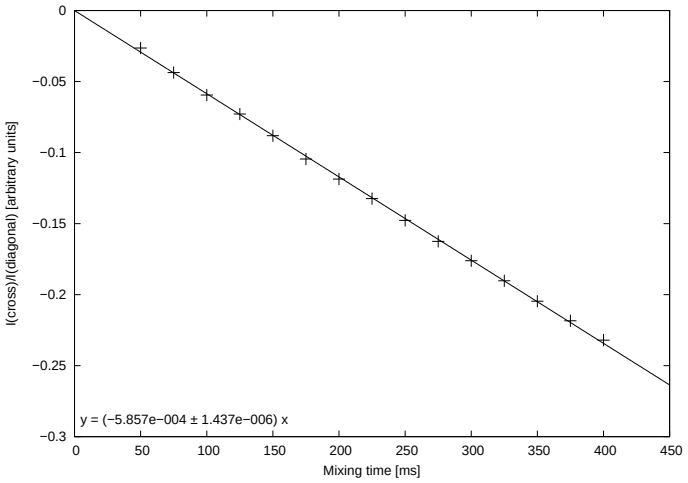

(y) H_{15a}–H_{15b} at 70% **1f1**

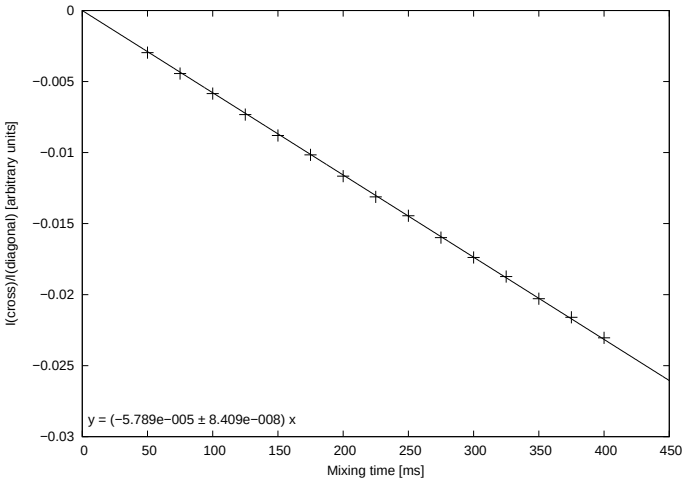

(z) H_{11b}–H_{23b} at 70% **1f1**

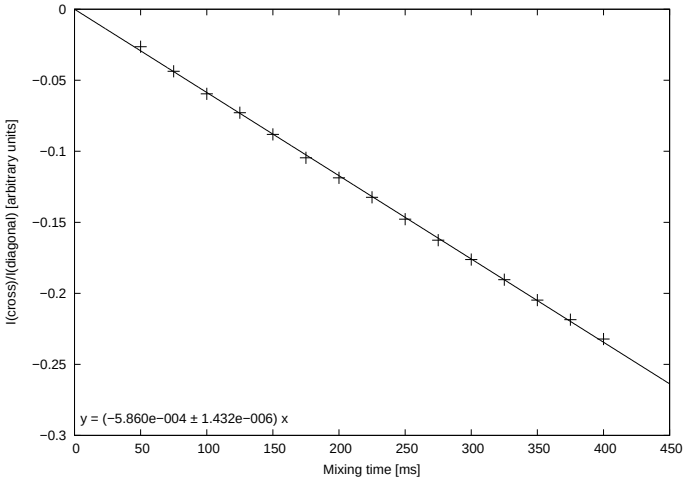

(aa) H_{15a}–H_{15b} at 60% **1f1**

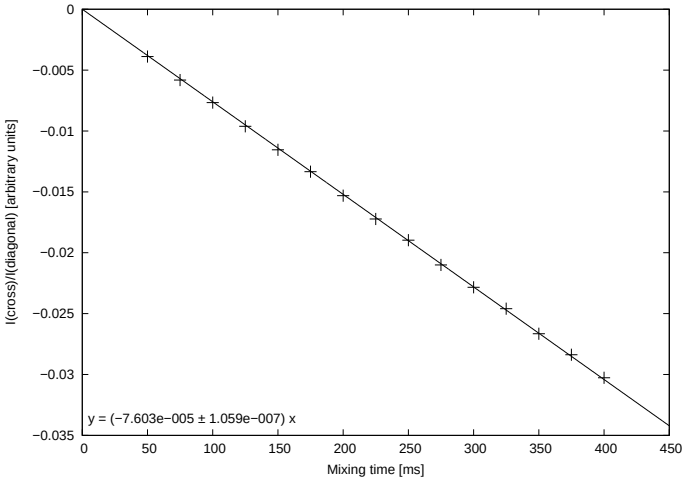

(ab) H_{11b}–H_{23b} at 60% **1f1**

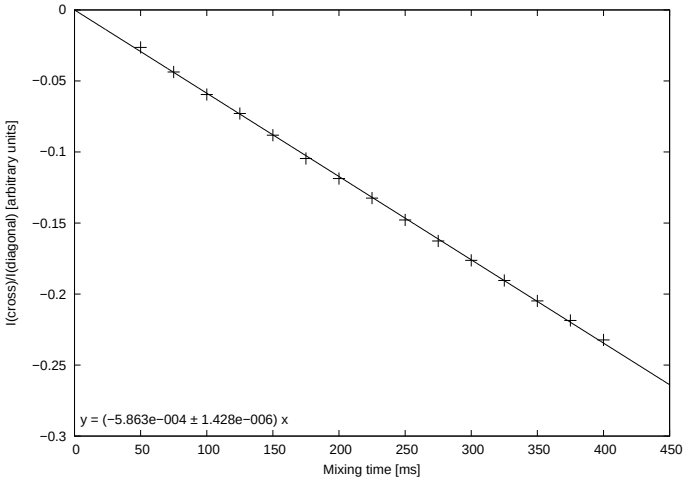

(ac) H_{15a}–H_{15b} at 50% **1f1**

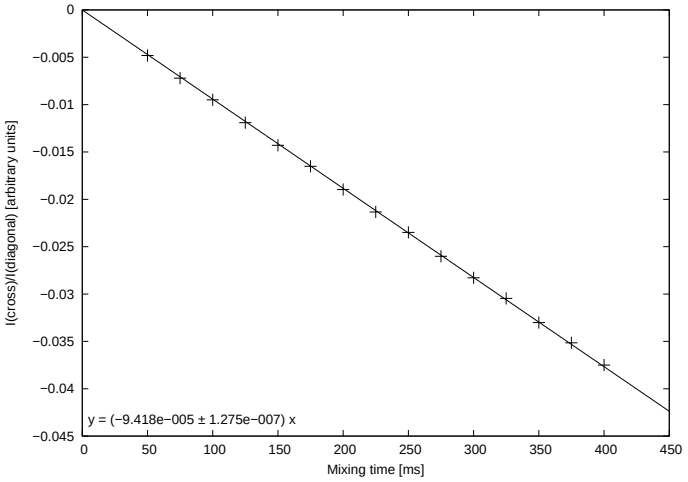

(ad) H_{11b}–H_{23b} at 50% **1f1**

Figure SI.11: The simulated PANIC plots for strychnine **1**.

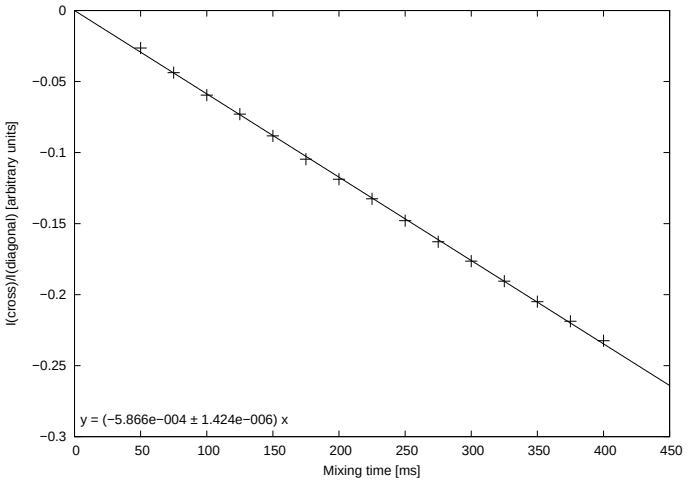

(ae) H_{15a}–H_{15b} at 40% **1f1**

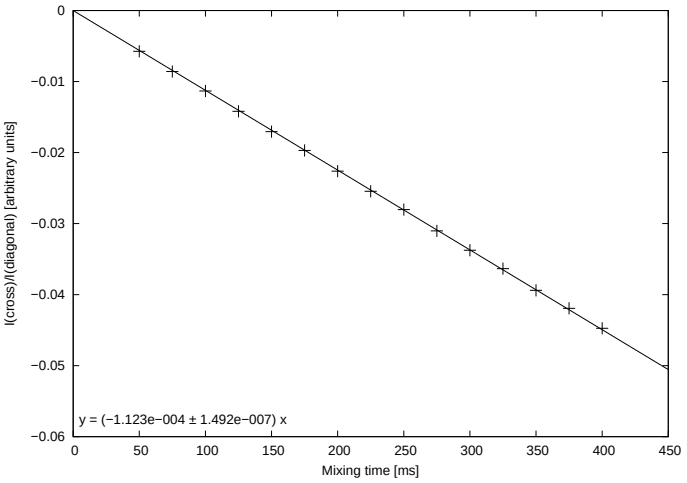

(af) H_{11b}–H_{23b} at 40% **1f1**

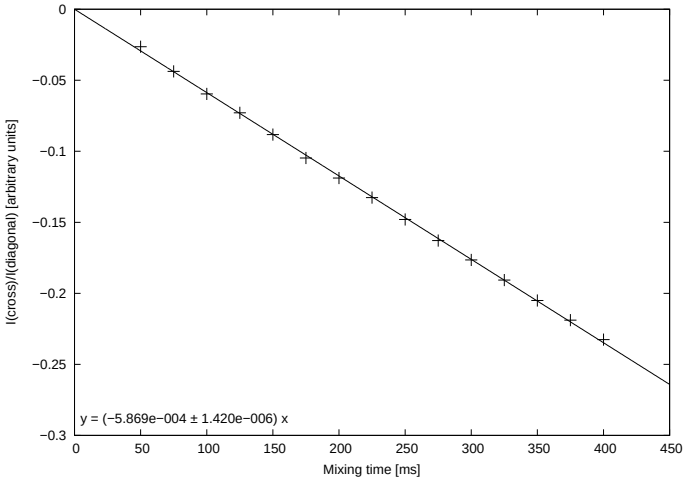

(ag) H_{15a}–H_{15b} at 30% **1f1**

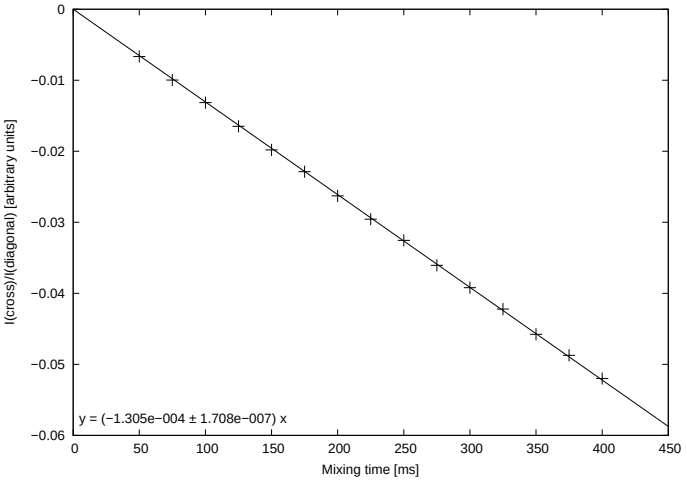

(ah) H_{11b}–H_{23b} at 30% **1f1**

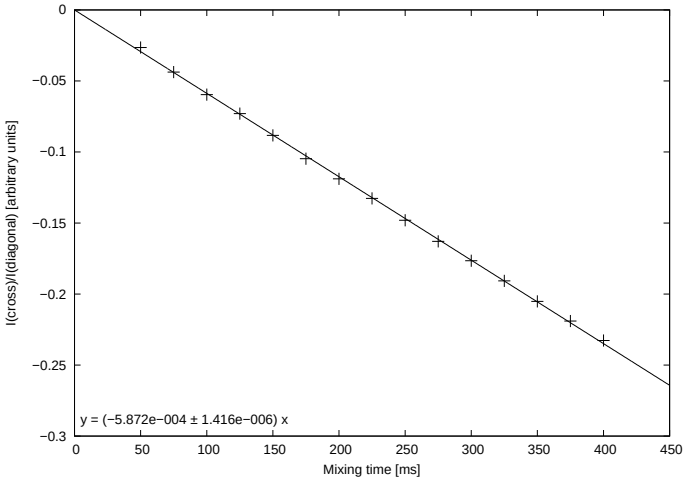

(ai) H_{15a}–H_{15b} at 20% **1f1**

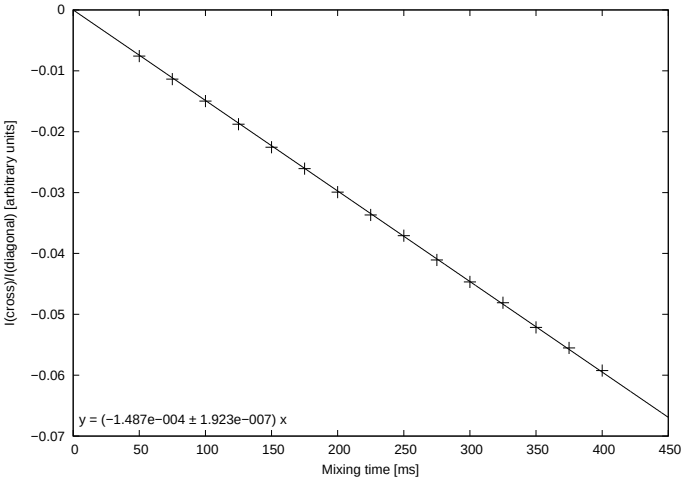

(aj) H_{11b}–H_{23b} at 20% **1f1**

Figure SI.11: The simulated PANIC plots for strychnine **1**.

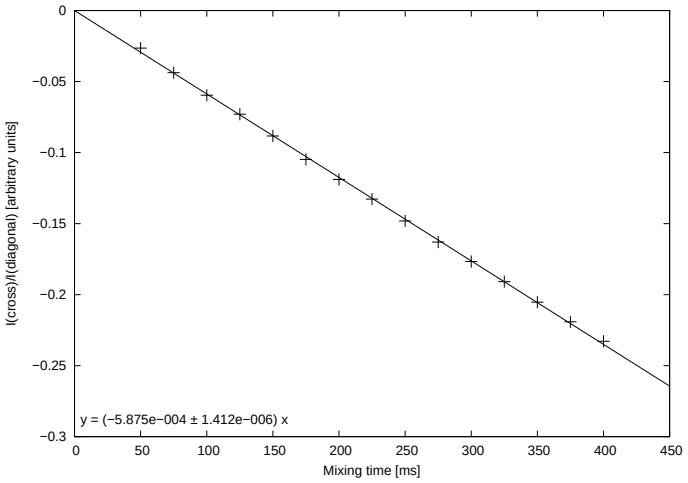

(ak) H_{15a}–H_{15b} at 10% **1f1**

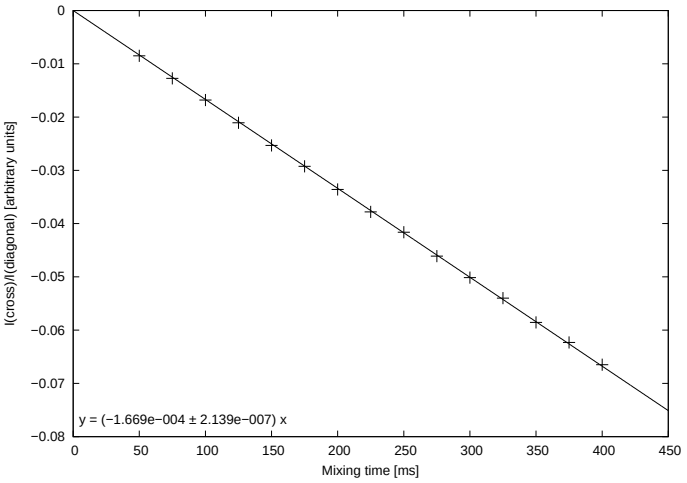

(al) H_{11b}–H_{23b} at 10% **1f1**

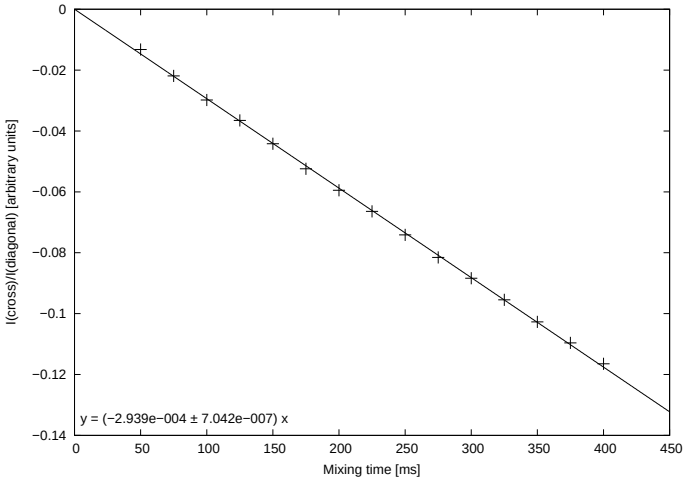

(am) H_{15a}–H_{15b} at 0% **1f1**

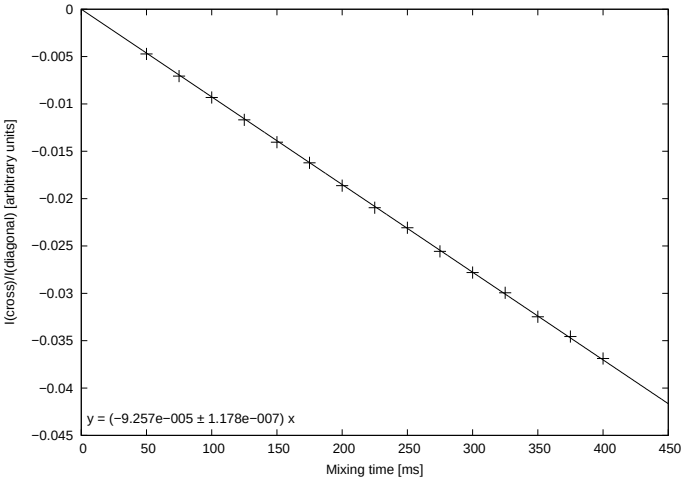

(an) H_{11b}–H_{23b} at 0% **1f1**

Figure SI.11: The simulated PANIC plots for strychnine **1**.

12. Literature

[1] J. Stonehouse, P. Adell, J. Keeler, A. J. Shaka, Ultrahigh-Quality NOE Spectra, J. Am. Chem. Soc. 116 (13) (1994) 6037–6038.

[2] K. Stott, J. Stonehouse, J. Keeler, T.-L. Hwang, A. J. Shaka, Excitation Sculpting in High-Resolution Nuclear Magnetic Resonance Spectroscopy: Application to Selective NOE Experiments, J. Am. Chem. Soc. 117 (14) (1995) 4199–4200.

[3] K. Stott, J. Keeler, Q. N. Van, A. J. Shaka, One-Dimensional NOE Experiments Using Pulsed Field Gradients, J. Magn. Reson. 125 (2) (1997) 302–324.

[4] M. J. Thrippleton, J. Keeler, Elimination of Zero-Quantum Interference in Two-Dimensional NMR Spectra, Angew. Chem. Int. Ed. 42 (33) (2003) 3938–3941.

[5] K. E. Cano, M. J. Thrippleton, J. Keeler, A. Shaka, Cascaded z-filters for efficient single-scan suppression of zero-quantum coherence, J. Magn. Reson. 167 (2) (2004) 291–297.

[6] M. J. Thrippleton, R. A. E. Edden, J. Keeler, Suppression of strong coupling artefacts in J-spectra, J. Mag. Reson. 174 (1) (2005) 97–109.

[7] H. Hu, K. Krishnamurthy, Revisiting the initial rate approximation in kinetic NOE measurements, J. Magn. Reson. 182 (1) (2006) 173–177.

[8] WEEDHEAD version 0.9.
URL `http://www.chemie.tu-darmstadt.de/thiele/forschung_9/nmrspektroskopie/methoden_2/weedhead/weedhead.en.jsp`

[9] C. P. Butts, C. R. Jones, E. C. Towers, J. L. Flynn, L. Appleby, N. J. Barron, Interproton distance determinations by NOE - surprising accuracy and precision in a rigid organic molecule, Org. Biomol. Chem. 9 (1) (2011) 177–184.

[10] C. M. Thiele, S. Berger, Probing the Diastereotopicity of Methylene Protons in Strychnine Using Residual Dipolar Couplings, Org. Lett. 5 (5) (2003) 705–708.

[11] C. M. Thiele, Simultaneous Assignment of All Diastereotopic Protons in Strychnine Using RDCs: PELG as Alignment Medium for Organic Molecules, J. Org. Chem. 69 (22) (2004) 7403–7413.

[12] B. Luy, K. Kobzar, H. Kessler, An Easy and Scalable Method for the Partial Alignment of Organic Molecules for Measuring Residual Dipolar Couplings, Angew. Chem. Int. Ed. 43 (9) (2004) 1092–1094.

[13] N.-C. Meyer, A. Krupp, V. Schmidts, C. M. Thiele, M. Reggelin, Polyacetylenes as Enantiodifferentiating Alignment Media, Angew. Chem. Int. Ed. 51 (33) (2012) 8334–8338.

[14] N. Meyer, Helikal chirale Polyacetylene in Katalyse und Analytik, Ph.D. thesis, TU Darmstadt (2012).

[15] H. J. Hogben, M. Krzystyniak, G. T. P. Charnock, P. Hore, I. Kuprov, Spinach - A software library for simulation of spin dynamics in large spin systems, J. Magn. Reson. 208 (2) (2011) 179–194.

[16] M. Hesse, H. Meier, B. Zeeh, S. Bienz, L. Bigler, T. Fox, Spektroskopische Methoden in der organischen Chemie, 8th Edition, Thieme, Stuttgart, 2011.

[17] S. Berger, D. Sicker, Classics in Spectroscopy: Isolation and Structure Elucidation of Natural Products, 1st Edition, Wiley-VCH Verlag GmbH & Co. KGaA, Weinheim, 2009.

[18] I. Kuprov, Diagonalization-free implementation of spin relaxation theory for large spin systems, J. Magn. Reson. 209 (1) (2011) 31–38.

[19] A. Karabanov, I. Kuprov, G. T. P. Charnock, A. van der Drift, L. J. Edwards, W. Köckenberger, On the accuracy of the state space restriction approximation for spin dynamics simulations, J. Chem. Phys. 135 (8) (2011) 084106.

[20] R. R. Ernst, G. Bodenhausen, A. Wokaun, Principles of Nuclear Magnetic Resonance in One and Two Dimensions, International Series of Monographs on Chemistry, Clarendon Press, 1990.

[21] J. Keeler, Understanding NMR Spectroscopy, 2nd Edition, Wiley, 2013.

[22] G. H. Meresi, M. Cuperlovic, W. E. Palke, J. Gerig, Pulsed Field Gradients in Simulations of One- and Two-Dimensional NMR Spectra, J. Magn. Reson. 137 (1) (1999) 186–195.

[23] P. Nicholas, D. Fushman, V. Ruchinsky, D. Cowburn, The Virtual NMR Spectrometer: A Computer Program for Efficient Simulation of NMR Experiments Involving Pulsed Field Gradients, J. Magn. Reson. 145 (2) (2000) 262–275.